Thermochemistry for enthalpies and reaction paths of nitrous acid isomers

3 AUTHORS:

Rubik Asatryan
University at Buffalo, The State University o…
51 PUBLICATIONS   365 CITATIONS

SEE PROFILE

Joseph W. Bozzelli
New Jersey Institute of Technology
277 PUBLICATIONS   5,260 CITATIONS

SEE PROFILE

John M. Simmie
National University of Ireland, Galway
148 PUBLICATIONS   3,491 CITATIONS

SEE PROFILE

Thermochemistry for Enthalpies and Reaction Paths of Nitrous Acid Isomers

RUBIK ASATRYAN,[1] JOSEPH W. BOZZELLI,[2] JOHN M. SIMMIE[2]

[1] Department of Chemistry and Environmental Science, New Jersey Institute of Technology, Newark, NJ 07102
[2] Department of Chemistry, National University of Ireland, Galway, Ireland

ABSTRACT: Recent studies show that nitrous acid, HONO, a significant precursor of the hydroxyl radical in the atmosphere, is formed during the photolysis of nitrogen dioxide in soils. The term nitrous acid is largely used interchangeably in the atmospheric literature, and the analytical methods employed do not often distinguish between the HONO structure (nitrous acid) and HNO_2 (nitryl hydride or isonitrous acid). The objective of this study is to determine the thermochemistry of the HNO_2 isomer, which has not been determined experimentally, and to evaluate its thermal and atmospheric stability relative to HONO. The thermochemistry of these isomers is also needed for reference and internal consistency in the calculation of larger nitrite and nitryl systems. We review, evaluate, and compare the thermochemical properties of several small nitric oxide and hydrogen nitrogen oxide molecules. The enthalpies of HONO and HNO_2 are calculated using computational chemistry with the following methods of analysis for the atomization, isomerization, and work reactions using closed- and open-shell reference molecules. Three high-level composite methods G3, CBS-QB3, and CBS-APNO are used for the computation of enthalpy. The enthalpy of formation, ΔH_f^o(298 K), for HONO is determined as -18.90 ± 0.05 kcal mol^{-1} (-79.08 ± 0.2 kJ mol^{-1}) and as -10.90 ± 0.05 kcal mol^{-1} (-45.61 ± 0.2 kJ mol^{-1}) for nitryl hydride (HNO_2), which is significantly higher than values used in recent NO_x combustion mechanisms. H-NO_2 is the weakest bond in isonitrous acid; but HNO_2 will isomerize to HONO with a similar barrier to the HO—NO bond energy; thus, it also serves as a source of OH in atmospheric chemistry. Kinetics of the isomerization is determined; a potential energy diagram of H/N/O_2 system is presented, and an analysis of the triplet surface is initiated. © 2007 Wiley Periodicals, Inc. Int J Chem Kinet 39: 378–398, 2007

INTRODUCTION

There are several stable structures for molecules whose formula is HONO or HNO_2; we use the following notation to distinguish individual species: *cis*- and *trans*-HONO for the isomers of nitrous acid, HNO_2 for isonitrous acid (nitryl hydride or hydrogen nitryl),

Correspondence to: J. W. Bozzelli; e-mail: Bozzelli@njit.edu.

cis- and *trans*-NHOO imine (nitrene) peroxides, *cis*- and *trans*-HOON hydroperoxynitrenes, HcyNOO for the cyclic dioxaziridine, and the term "HONO-isomers" for the grouping of HONO-*cis* and HONO-*trans* plus HNO_2.

HONO plays an important role in urban and in remote atmospheric chemistry in the stratosphere and in the troposphere [1–4], where it is recently reported to be emitted into the atmosphere from the photochemical processes involving NO_2 in soils [1a]. The moderately weak HO—NO bond (49 kcal mol^{-1}) is a source of OH-radicals and is considered to be the daytime regulator for oxidation capacity in the atmosphere. Recent field measurements in Rome [2a] confirm that HONO photolysis is the most important primary OH source in the lowest part of the troposphere during the first hours after sunrise, when hydroxyl radical production rates from the photolysis of ozone and formaldehyde are slow. HONO is reported to be involved in the formation of atmospheric aerosols, soot particles, and atmospheric pollution processes [1b,3,4]. HONO is also a well-known generator of the NO^+ electrophile in synthetic organic chemistry, and its significance in biomedicine and toxicology is also well established [5,6]. Human health implications from indoor levels of HONO have recently been recognized [7].

Until recently, it was believed [1a] that HONO was mainly formed by heterogeneous reaction on surfaces in the presence of water according to the overall reaction of $H_2O + 2NO_2 \rightarrow HNO_3 + HONO$ (an alternate set of products, $HNO_3 + HNO_2$ are also suggested) [4]. The photosensitized reduction of NO_2 on the surfaces of soil, peat, and other environmental substances containing humic acid is suggested to result in a complex mélange of phenoxy-type macromolecules. It is hypothesized here that the major role of these partly oxidized aromatic intermediates gives off HONO in the lowermost region of the troposphere [1a,8,9].

Other sources of HONO include the photodissociation of nitric acid [10] to form HONO $+O(^3P)$ and H-abstraction reactions from methane and nonmethane hydrocarbons by NO_2. HONO is also formed from unimolecular dissociation (concerted HONO molecular elimination) from organic nitrates, nitrites, and nitroalkanes (nitroparaffins) etc. [1,3,4,11,12].

The most important sink of HONO in the atmosphere is photolysis to OH + NO and H + NO_2 radicals [13,14]. In combustion and other thermal processes, the important loss mechanism is due to unimolecular dissociation of HONO via cleavage of the weak HO—NO bond.

HONO is known to be an important intermediate in combustion processes where nitrogen oxides are present. The mechanisms leading to its formation and the role of HONO isomers in these reaction mechanisms are not, however, completely understood [11,12,15–17].

HONO is the simplest model and is a prototype of organic nitrites; its nitroform isomer HNO_2 can be considered a prototype of nitrocompounds as well. HONO is also one of the simpler systems that undergo cis–trans isomerism, and this feature is responsible for a number of literature studies on nitrous acid.

Isomers of HONO

The potential energy surface of the HONO isomers includes five high-energy isomers and three moderately stable isomers, which include *trans*-HONO, *cis*-HONO, and the nitroform HNO_2. Figure 1 illustrates the structure of each isomer.

The vibration frequencies and structures of the *trans*- and *cis*-HONO isomers are known from both experimental and theoretical studies [18–45]. The potential energy surface (PES) for HONO (cis–trans isomerization and decomposition pathways) has been theoretically examined in some detail [18–27,37,42] with an experimentally reported [28a,42,43] barrier to isomerization of 8.7–11.5 kcal mol^{-1}.

The trans conformation of HONO (or *E*-isomer) appears to be a global minimum on the PES of all the HONO isomers [34,34a,37,40a,42]. The next most stable isomers (on an enthalpy of formation scale) are, respectively *cis*-HONO (or *Z*-isomer) and HNO_2 of C_{2v} symmetry, see Fig. 1a and Tables I and II.

Sengupta et al. [21] have recently reported the structure and stability of ionic and neutral *trans*-HONO; the dissociation of neutral *trans*-HONO to OH + NO radicals was calculated to be 45.9 kcal mol^{-1} with the B3LYP/6–311++G(3df,2pd) method, whereas current thermochemistry (Table I) suggests a value of 49 kcal mol^{-1} for this dissociation (vide infra).

Cis- and trans- Isomers of HONO are isoenergetic, but the trans form is dominant in the gas phase and is slightly preferred by 0.4 kcal mol^{-1} according to infrared spectrometry [28] and by 0.37 kcal mol^{-1} from microwave spectroscopy [29]. Important experimental data [43a] on the barrier of cis–trans isomerization of HONO in the rare gas, low-temperature matrix study by De Maré and Moussaoui [42], resulting in a value of 9.3 kcal mol^{-1}. Proton-mediated tunneling effects are indicated to play a major role here [41,43a], where the cis to trans isomerism was reported to be much faster than the reverse interconversion [41b].

Heats of Formation

The experimental data for the heat of formation, ΔH_f^o (298K), of *trans*-HONO was evaluated by Chase [48]
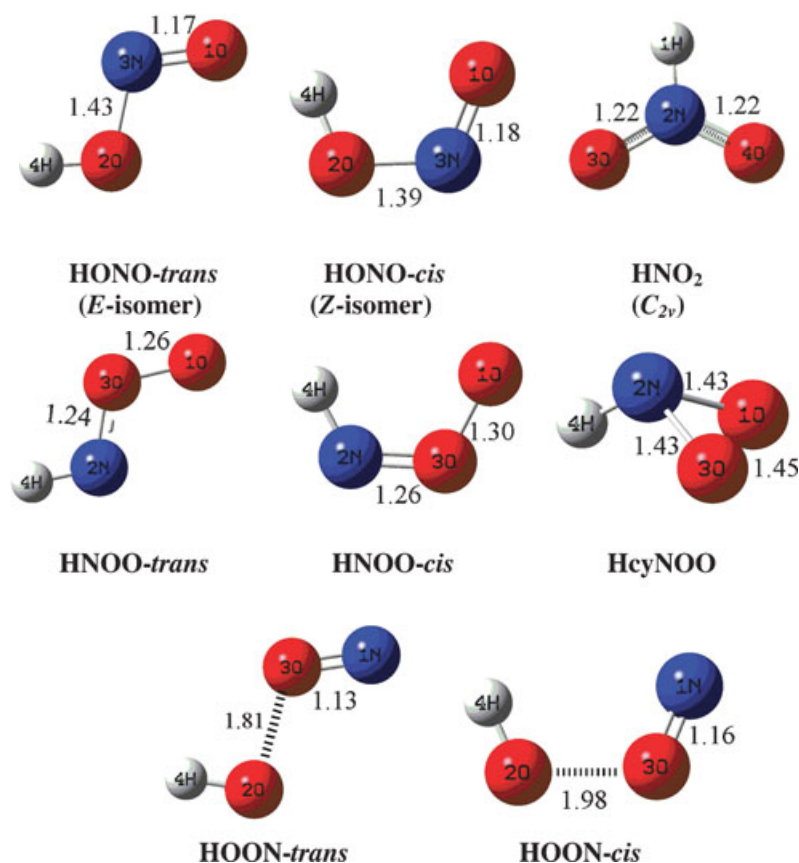
Figure 1   (a) Illustration of most stable HONO isomers (see Table II for details). (b) High-energetic HONO isomers. [Color figure can be viewed in the online issue, which is available at www.interscience.wiley.com.]

at -18.84 kcal mol^{-1} and by Gurvich et al. [49] at -18.87 kcal mol^{-1}. A value of -18.3 for the cis isomer was listed by Benson [50], and -18.34 kcal mol^{-1} and -18.51 kcal mol^{-1} by Chase [48] and Gurvich et al., [49], respectively.

The BAC-MP4 calculated heat of formation of *trans*-HONO by Melius [37] is -17.68 kcal mol^{-1}, which is 1.4 kcal mol^{-1} higher in energy than the calculated heat of formation for the cis isomer of -19.11 kcal mol^{-1}. The BAC-MP4 heat of formation for the HNO$_2$ isomer is -14.15 kcal mol^{-1}, which is only slightly higher than the BAC-MP4 value for *trans*-HONO.

The enthalpy of formation for HONO has been more recently studied by Jursic using the atomization energy technique at the CBSQ and DFT levels [19]; he report that the best calculated value is -18.4 kcal mol^{-1} at 0 K (-19.9 at 298 K; see Appendix B), from the CBSQ level. The CBS-QB3 method was recently used by Sumathi et al. [22] for estimating $\Delta H_{\rm f}^{\rm o}$ (298 K) for the trans isomer of nitrous acid in both the gas phase and in solution (the Polarized Continuum model and the integral equation formalism were employed for the solvent heats of atomization). Their estimated values

were -18.33 kcal mol^{-1} and -23.17 kcal mol^{-1}, respectively for gas and liquid-phase *trans*-HONO. Calculations on proton affinity and ionization energy cycles for HONO at the CCSD(T) level suggested the value of -16.8 kcal mol^{-1}; this is almost the same value determined from the HNO + H$_2$O $\rightarrow$ HNO$_2$ + H$_2$ exchange reaction (16.7 kcal mol^{-1}) [23].

An experimental benchmark value for the heat of formation of the trans isomer of nitrous acid is further evaluated in this study. Our results agree with the value (-18.87) that Gurvich et al. recommend [49], and we have chosen $\Delta H_{\rm f}^{\rm o}$ (298 K) $= -18.87$ kcal mol^{-1} for *trans*-HONO as the correct value and appropriate for further use as a reference.

This HO—NO bond energy has also been studied using both DFT and higher level methods [19,24,25]. Bauerfeldt et al. [24] have computed the bond dissociation energy of *trans*-HONO(X^{1}A$'$) $\rightarrow$ HO(X^{2}P) + NO(X^{2}P) theoretically with a number of different methods and concluded that the best agreement with the experimental 49.2 kcal mol^{-1} value [46] can be obtained with a B3LYP/6–311G(3d2f,3p2d) value of 49.0 kcal mol^{-1}.

Table I Experimental and Calculated Heats of Formation (kcal mol^{-1}) for Species Data in Bold are Recommended, Used in Work Reactions and Evaluations[a]

Species	Experimental ΔH_f^o (298)	Calculated ΔH_f^o (298)
NO	**21.76** [76], 21.58 [46]	22.3 [70][d]
NO$_2$	**7.91** [46], 8.12 [76]	
HNO	**25.6** [46], 23.8 [48]	23.20 [37], 25.41 [16], 26.1 [70]
HONO-*trans*	−**18.87** [49]	−18.33 [22]
	−18.84 [48]	−18.59 [16]
	−17.68 ± 1.00 [37]	−**18.9 ± 0.05** [this work][e]
HONO-*cis*	−**18.34** [48], −18.3[b] [50]	−19.11 ± 1.12 [37]
		−**18.4** ($\Delta H_i = 0.46$ kcal/mol) [this work]
HNO$_2$	. . . .	−14.15 ± 1.4 [37]
		−**10.9 ± 0.05** [this work]
HOON-*trans*		39.34 [37]
HOON-*cis*		46.42 [37]
HNOO-*trans*		56.28 [16], 57.07 [37]
HNOO-*cis*		54.56 [37]
HcyNOO		65.01 [37]
HONO$_2$	−**32.10** [46]	−32.15 [22]
	−32.0 ± 0.1 [49]	
CH$_3$NO$_2$	−19.30 ± 0.3 [46]	−17.65 [51]
	−**17.86 ± 0.15** [46][e]	
	−17.8 ± 0.2 [72,73]	
	−17.9 [50], −13.6 ± 0.3 [46]	
CH$_3$ONO	−**15.64 ± 0.20** [46]	−15.64 [51]
	−15.79 ± 0.25 [46][e]	
	−16.8 ± 0.8 [46]	
	−14.93 ± 0.26 [46]	
	−15.6 [50], −15.3 [74]	
CH$_3$OH	−**48.04** [46]	
CH$_3$OCH$_3$	−**43.99 ± 0.12** [48]	
H	**52.103** [46], 52.64 = 51.63 ± 0.001 (1.01) [67][f]	
O	**59.555** [46], 60.03 = 58.99 ± 0.02(1.04) [67][f]	
C	**171.29** [46], 170.23 = 169.98 ± 0.1 (0.25) [67][f]	
N	**112.97** [46], 113.57 = 112.53 ± 0.02 (1.04) [67][f]	
HCO	**10.4** [48]	
CH$_2$O	−**26.05** [52], −25.98 [46]	
H$_2$O	−**57.7978** [75]	

[a] Data in bold are recommended, used in evaluations and in work reactions.

[b] Originally: HONO-*cis* [50, Table A.10].

[c] Recalculated for $T = 298$ K value by adding thermal coefficient −1.51 kcal/mol to ΔH_f^o (0 K) of HNO$_2$ and *trans*-HONO, see text.

[d] Based on the average bond dissociation values.

[e] Recommended by Cox and Pilcher, comprehensive review [80].

[f] ΔH_f^o (0 K) for atoms and corresponding temperature corrections (in parenthesis) [66,67] are used for comparison.
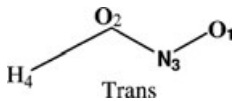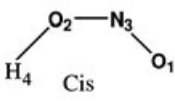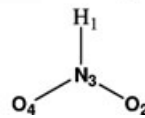
A recent experimental study has reported the dissociation energy of the HO—NO bond as 48.01 kcal mol^{-1} (16,772 ± 14 cm^{-1}) using double-resonance overtone photofragment spectroscopy [44].

HNO$_2$ Isomer–Hydrogen Nitryl

We have not found widely referenced importance assigned to the HNO$_2$ structure, and this probably ex-

plains why it is not as well studied as the HONO forms. HNO$_2$ is, however, thermally more stable than the HONO isomers with the weakest bond H—NO$_2$ at 70 kcal mol^{-1} relative to the HO—NO bond at 49 kcal mol^{-1} (HNO$_2$ does isomerize to HONO over a low barrier, and it also serves as a source of OH in atmospheric chemistry via the isomerization–HONO dissociation path). The HNO$_2$ isomer has recently been observed in matrix isolated nitric acid photolysis in combination

**Table II** Geometry and Enthalpy of HONO Isomers vs. Calculation Method[a]

	Distances (Å)			Angles (deg)		
Method	1–3	2–3	2–4	1–3–2	3–2–4	Enthalpy[b] (au)
trans-HONO (*trans*-Nitrous Acid)						
B3LYP/6–31G(d,p)	1.1787	1.4266	0.9724	102.4	110.6	−205.675762
B3LYP/6–31+G(2d,2p)	1.1687	1.4280	0.9698	102.7	111.1	−205.701551
B3LYP/6–311++G(3df,2p)	1.1629	1.4277	0.9678	102.9	111.1	−205.761577
CBS-QB3//B3LYP/6–31 lG(2d,d,p)	1.1663	1.4331	0.9677	102.3	111.1	−205.470808
CBS-APNO//QCISD/6–311G(d,p)	1.1723	1.4125	0.9630	101.9	110.8	−205.680733
G3//MP2(Full)6–31G(d)	1.1968	1.4226	0.9796	101.9	110.4	−205.598921
QCISD(T)/6–311++G(2df,2p)[c]	1.174	1.425	0.967	102.1	111.8	—
QCISD(T)/6–311++G(3df,3pd)[d]	1.173	1.427	0.966	101.9	110.8	—
Experimental[e]	1.173	1.441	0.947	102.1	110.5	—
Experimental[f]	1.170	1.432	0.958	102.1	110.7	—
Experimental[g]	1.177	1.433	0.954	102.1	110.7	—
cis-HONO (*cis*-Nitrous Acid)						
B3LYP/6–31G(d,p)	1.1918	1.3846	0.9832	105.5	113.2	−205.677240
B3LYP/6–31+G(2d,2p)	1.1822	1.3885	0.9801	106.3	113.8	−205.700798
B3LYP/6–311++G(3df,2p)	1.1765	1.3875	0.9783	106.4	113.8	−205.760790
CBS-QB3//B3LYP/6–31 lG(2d,d,p)	1.1805	1.3882	0.9793	105.9	113.6	−205.470243
CBS-APNO//QCISD/6–31 G(d,p)	1.1837	1.3794	0.9731	104.5	113.1	−205.679981
G3//MP2(Full)/6–31 G(d)	1.2094	1.3853	0.9909	104.5	112.8	−205.598006
QCISD(T)/6–311++G(2df,2p)[c]	1.186	1.390	0.976	104.8	113.5	—
QCISD(T)/6–311++G(3df,3pd)[d]	1.186	1.392	0.976	104.6	113.2	—
Experimental[e]	1.190	1.397	0.975	104.4	113.5	—
Experimental[f]	1.185	1.392	0.982	104.0	113.6	—
HNO$_2$ (isoNitrous Acid, Nitryl Hydride, Hydrogen Nitryl)						
B3LYP/6–31G(d,p)	1.0438	1.2223	1.2223[g]	115.8	128.4[h]	−205.663815
B3LYP/6–31+G(2d,2p)	1.0411	1.2174	1.2174[g]	115.9	128.2[h]	−205.690769
B3LYP/6–311++G(3df,2p)	1.0415	1.2130	1.2130[g]	115.8	128.3[h]	−205.750639
CBS-QB3//B3LYP/6–31 lG(2d,d,p)	1.0441	1.2150	1.2150[g]	115.7	128.5[h]	−205.458280
CBS-APNO//QCISD/6–311G(d,p)	1.0380	1.2142	1.2142[g]	115.8	128.4[h]	−205.667684
G3//MP2(Full)6–31G(d)	1.0399	1.2363	1.2363[g]	115.8	128.4[h]	−205.586271
QCISD/6–311++G(d,p)[i]	1.038	1.216	1.216[g]	115.9	128.2[h]	—
QCISD/6–311++G(2df,2p)[j]	1.033	1.211	1.211[g]	115.8	128.3[h]	—

[a] Final geometry for composite methods is determined by methods after double slash.

[b] Final enthalpy of composite and single methods; ZPVE and thermal corrections are included.

[c] Calculation results from [25].

[d] From Francisco [45].

[e] From Finnigan et al. [30a].

[f] From Cox et al. [30b].

[g] Distance N3-O4.

[h] Angle O2-N3-O4.

[i] From Ling et al. [34].

[j] From Chan and coworkers [20].

with FTIR spectroscopy [10]. HNO$_2$ can be formed via abstraction of weakly bound hydrogen atoms by NO$_2$ similar to formation of HONO, but the significance of this channel is dependent on the H—NO$_2$ bond energy. Abstraction from HNO is clearly exothermic (HNO + NO$_2$ → HNO$_2$ + NO). Disproportionation reactions

are other formation paths for HNO_2:

$$NO_2 + HO_2 = HNO_2 + O_2$$

and

$$NO_2 + CCO^{\bullet} \text{ (alkoxy radical)} \leftrightarrows HNO_2 + CCH(=O)$$
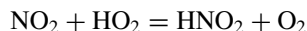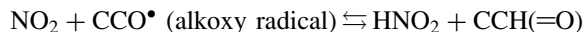
A potential energy surface of anionic, cationic, and neutral nitrous acids has been developed by Sumathi over several collaborations [21–23]. Nguyen et al. [23] have calculated the isomerization barrier of HONO to HNO_2 ($E_a = 55.8$ kcal mol^{-1}) as well as two high-energy conversions of the cyclic isomer to HNO_2 and HNOO (at the 110 and 120 kcal mol^{-1} levels relative to

OH + NO reagents, respectively) in the neutral system using DFT and CCSD(T) methods.

HNO_2 is not considered to be formed from HONO via an isomerization process, because the isomerization barrier of 55.8 kcal mol^{-1} is higher than the HO−NO bond energy and it is too high to occur under atmospheric conditions [19a,23,37,38a]. The high barrier is further supported by the similar barriers for isomerization to organonitrates from the corresponding nitrites [3,31,33] for gas phase, nonhydrated reactions.

HNO_2 is known to be an important intermediate from models of nitrogen chemistry that are in combustion models [16]. The reaction of $^3NH + O_2$ is reported to form HNOO, which isomerizes to both HONO and

Table III Vibrational Frequencies (cm^{-1}) and Moments of Inertia (au) of HONO Isomers vs. Calculation Method[a]

| Method | Frequency (cm^{-1}) | | | | | | Moments of Inertia (amu) | | |
	v6	v5	v4	v3	v2	vl	I_1	I_2	I_1
trans-HONO	a''	a'	a'	a'	a'	a'			
B3LYP/6–31G(d,p)	594.2	630.9	861.8	1305.4	1791.9	3757.5	19.51425	143.64687	163.16111
B3LYP/6–31+G(2d,2p)	587.9	622.5	821.7	1310.3	1776.9	3767.4	19.14305	143.58962	162.73267
B3LYP/6–311++G(3df,2p)	590.3	620.9	818.9	1302.9	1782.4	3772.2	18.99956	143.13000	162.12956
CBS-QB3//B3LYP/6–311G(2d,d,p)	590.8	619.0	834.1	1297.7	1792.4	3776.2	19.18510	143.84019	163.02529
CBS-APNO//HF/6–311G(d,p)	588.1	800.3	1088.6	1498.0	2040.5	4146.1	17.34547	132.69472	150.04018
G3//HF/6–31G(d)	599.9	790.7	1099.5	1514.4	2042.9	4081.3	17.69577	133.46480	151.16057
QCISD/6–311+G(d)[b]	543	658	858	1342	1781	3838			
QCISD/6–311++G(2df ,2p)[c]	568	665	868	1350	1777	3833			
QCISD/6–311++G(2df ,2p)[c,d]	—	—	—	1275	1713	3674			
QCISD(T)/6–31G(d)[e]	583	608	838	1323	1720	3667			
HF/4-31G(d)[f]	530	700	970	1350	1820	3620			
Experiment[g]	—	593	791	1265	1699	—			
Experiment[h]	543.0	595.6	790.1	1263.2	1699.8	3590.7			
Experiment[b]	—	628?	813	1310	1680	3498			
Experiment[i]	—	702	801	1421	1635	3512			
Experiment[j]	583	625	815	1298	1684	3558			
Experiment[k]	—	—	816.4	1293.7	1677.6	3510.9			
cis-HONO	a''	a'	a'	a'	a'	a'			
B3LYP/6–31G(d,p)	648.1	735.3	922.0	1349.3	1725.7	3579.8	21.65233	135.88761	157.53994
B3LYP/6–31+G(2d,2p)	634.5	691.7	880.9	1345.2	1710.0	3597.5	21.25693	136.48280	157.73972
B3LYP/6–311++G(3df,2p)	635.1	694.3	875.9	1341.4	1715.8	3597.7	21.11928	135.89830	157.01756
CBS-QB3//B3LYP/6–311G(2d,d,p)	638.6	716.6	892.8	1337.7	1720.2	3586.8	21.28061	135.97558	157.25618
CBS-APNO//HF/6–311G(d,p)	727.8	791.6	1155.1	1521.7	1983.0	3997.1	19.85564	126.73047	146.58612
G3//HF/6–31G(d)	746.4	784.4	1160.9	1542.4	1987.7	3939.5	20.19293	127.52289	147.71582
QCISD/6–311++G(2df,2p)[c]	672	674	928	1382	1722	3686			
QCISD/6–311++G(2df,2p)[c,d]	—	—	—	—	1652	3520			
QCISD(T)/6–31G(d)[e]	718	634	898	1367	1667	3512			
HF/4–31G(d)[f]	670	700	1030	1370	1770	3490			
Experiment[h]	638.5	609.0	851.9	—	1640.5	3426.2			
Experiment[k]			869.4	—	1629.9	3404.0			
Experiment[g]	—	608	853	1261	1640	—			
Experiment[h]	—	628?	868	—	1625	3360			
Experiment[i]	—	721	857	—	1611	—			
Experiment[j]	658	—	865	—	1633	3410			

Continued

Table III *Continued*

Method	Frequency (cm^{-1})						Moments of Inertia (amu)		
	v6	v5	v4	v3	v2	vl	I_1	I_2	I_1
HNO$_2$	a'	a'	a'	a''	a''	a'			
B3LYP/6–31G(d,p)	782.5	1049.9	1414.2	1520.2	1701.8	3170.8	16.87025	138.38335	155.25360
B3LYP/6–31+G(2d,2p)	787.0	1049.0	1407.5	1515.6	1651.9	3200.0	16.83914	137.01294	153.85207
B3LYP/6–311++G(3df,2p)	795.8	1058.5	1409.2	1513.3	1647.7	3176.9	16.72086	136.13373	152.85459
CBS-QB3//B3LYP/6–311G(2d,d,p)	800.3	1068.2	1407.8	1542.4	1677.3	3147.0	16.68753	136.87070	153.55823
CBS-APNO//HF/6–311G(d,p)	899.6	1244.5	1627.7	1703.6	1914.9	3517.9	15.82633	128.93837	144.76470
G3//HF/6–31G(d)	881.2	1229.1	1629.8	1691.1	1934.5	3575.1	15.92335	130.46894	146.39229
QCISD/6-311+G(d)[b]	800	1078	1418	1561	1665	3278			
QCISD/6–311++G(2df,2p)[c]	803	1085	1425	1536	1666	3310			
QCISD/6–311++G(2df,2p)[c,d]	750	—	1325	1633	—	—			
Experiment[j]	792	1016	1376	weak	1600	3289			
Experiment[b]	834	924	1372	weak	1605	3137			

[a] For composite methods frequency is determined by methods after double slash.
[b] From Ling et al. [34].
[c] From Chan et al. [20].
[d] Corrected to anharmonisity.
[e] From Francisco [45].
[f] From Nakamura et al. [40a]
[g] From McGraw et al. [28a].
[h] From Deeley et al. [28b].
[i] From McDonald et al. [43b].
[j] From Ruscic et al. [76].
[k] From Koch and Sodeau [10].

HNO$_2$ with subsequent dissociation reactions to OH + NO and H + NO$_2$, respectively [16,38]. The results of isomerization reactions and reaction to stabilized adducts versus further dissociation are sensitive to the isomerization barriers and thermochemistry of the respective species [16,37b] as well as pressure and temperature.
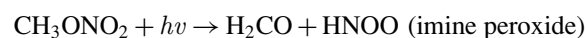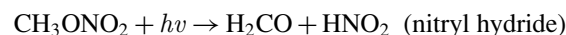
The research groups of H. Pritchard and M. C. Lin as well as Yamaguchi et al. have used calculations to study HONO formation via abstraction reactions, where the formation of isonitrous acid HNO$_2$ is included [20,27b,c,d]. Inferences of its enthalpy come from their reported reaction energies, where NO$_2$ abstracts a hydrogen atom from HBr, HI, CH$_2$O, H$_2$, H$_2$S, H$_2$O, CH$_3$OH, HONO [20] and from NH$_3$ [27c]. These groups show ΔH_{rxn} to HNO$_2$ is about 7.7–9.2 kcal mol^{-1} higher than to HONO. Chan and Pritchard also used calculations to study the disproportionation reaction of NO$_2$ + HO$_2$ to HNO$_2$ + O$_2$, which is 22.7 kcal mol^{-1} exothermic but they report [20a] a barrier of 10 kcal mol^{-1}. This barrier seems high; but may be the reason the HNO$_2$ path is not competitive with the association reaction (HO$_2$ + NO$_2$ → HOONO$_2$ → OH + NO$_3$) and is why the formation of HNO$_2$/HONO is not observed in low-temperature or high-pressure experiments [47].

The hydrogen nitryl (HNO$_2$ form of nitrous acid) has been shown to be an alternative structural model

for the donor–acceptor complex ammonium nitrite, NH$_4$NO$_2$, which is the simpler model of the highly energetic material ammonium dinitramide, NH$_4$N(NO$_2$)$_2$ [53].

There is some evidence indicating the HNO$_2$ isomer is a stabilizing species in the NO–(CH$_3$)$_3$CO$^\bullet$ system as discussed recently by Zhao et al. [54] Furthermore, Hug et al. [55] have observed and characterized the HNO$_2^{\bullet-}$ radical anion by electron paramagnetic resonance spectroscopy with further support from quantum chemical calculations. The radiolytic yield of HNO$_2^{\bullet-}$ radical anion form was shown to be dominant, in spite of the fact that it is ~10 kcal mol^{-1} less stable, relative to the nitrous acid form HONO$^{\bullet-}$.

While the thermal decomposition of nitrates is mainly attributed to HONO formation [3], the primary photochemical products of CH$_3$ONO$_2$ degradation from 266 nm photons are reported to be HNO$_2$ and HNOO isomers [34]:

CH$_3$ONO$_2$ + $h\nu$ → H$_2$CO + HNO$_2$ (nitryl hydride)

CH$_3$ONO$_2$ + $h\nu$ → H$_2$CO + HNOO (imine peroxide)

The branching ratio between two channels above is reported to be close to unity. The HONO isomers (both cis and trans) are reportedly formed in secondary processes. The observation of the HNO$_2$ isomer here is

consistent with its higher overall stability. HNO_2 was reported to be a secondary product from $HONO_2$ photolysis in an argon matrix [10].

The recombination $HONO + O(^3P)$ to produce nitric acid, which is a sink for NO_x, is less likely to proceed for HNO_2, since all electrons on the central atom of HNO_2 are involved in bonding, unlike the thermodynamically more stable linear cis- and trans-HONO isomers.

Matrix studies [56] have reported that only cis- and trans-HONO are produced in the reaction $H + NO_2$ despite the theoretical prediction [57], which suggested that HNO_2 should be formed rather than HONO.

Thermochemical properties on the HNO_2 isomer are needed to evaluate its importance and to use it as a reference molecule in comparison enthalpy evaluations (work reactions, vide infra) and for validating computational chemistry. To our knowledge, the thermochemistry of this HNO_2 isomer has not been experimentally determined, although it has been partly analyzed via theoretical methods [19,20,23,37,39]. The ΔH_f^o (298 K) of HNO_2 is −14.15 kcal mol^{-1} according to BAC-MP4 calculations [37], and this value is in use in the Chemkin thermochemical database [58a] and in kinetic mechanisms on NO acceleration of hydrocarbon combustion by a number of research groups: Bromley et al. [58b] and Roesler and co-workers [58c]. A lower enthalpy, −17.4 kcal mol^{-1}, is used in the Utah group mechanisms of Djurazic [58d] that is not significantly different from that of HONO.

Nguyen et al. have reported value of ΔH_f^o (298 K) $= −8.5 \pm 2$ kcal mol^{-1} using the CCSD(T) ab initio method [23]. Takane and Fueno used CASSCF and other multireference methods [39] estimated that the HNO_2 isomer is 15.78 kcal mol^{-1} higher in enthalpy than the HONO-trans isomer. A value of −18 for trans-HONO places $\Delta H_{f(298\ K)}^o$ HNO_2 at −2.5 kcal mol^{-1}.

The enthalpy of formation of HNO_2 (0 K) reported by Jursic is −10 kcal mol^{-1}. We use heat of atomization from the CBSQ composite method [19b] to compare this value with experiment and with our calculated data at 298 K. We determine and use a temperature correction (0–298 K) of −1.51, placing his value at −11.5 kcal mol^{-1} (see Appendix B and Table I).

Jursic also reported values from G1, G2, and G2MP2 composite methods that predicted higher stability of both the trans-HONO and the HNO_2 isomers than were determined with the CBSQ method. Estimated values at the G1, G2, and G2MP2 levels are −13.3, −14.5, and −15.3 kcal mol^{-1} for HNO_2, and −21.9, −22.9, and −24.1 (all converted to 298 K) for trans-HONO, respectively. Jursic chose the CBSQ results as the best values. The best agreement of Jursic's CBSQ enthalpy, −11.5 kcal

mol^{-1} (298 K), for HNO_2 in his DFT method studies was at the B3LYP/6–311G(3df,3pd) level; it resulted in −11.1 kcal mol^{-1} at 298 K, using the atomization procedure [19a].

Chan and Pritchard reported an enthalpy difference between HNO_2 vs. HONO as 8.5 and 8.1 kcal mol^{-1} at CCSD(T)/6–311G(d,p)//BHandHLYP/6–311G(d,p) and BHandHLYP/6–311G(d,p) levels [20]. These authors acknowledge that both calculations incorrectly predict the cis to be more stable than the trans-HONO isomer. The authors found that use of an extended basis set, 6–311G++(2df,2p), predicted the correct stability. The barrier for conversion between HONO rotational isomers is also overestimated in the CCSD(T) and BHandHLYP calculations at 11.7 and 15.9 kcal mol^{-1} vs. experimental 8.7–10 kcal mol^{-1}.

The data above illustrate that there is considerable variation in reported values for HNO_2 and in several other isomers. A systematic study using several high-level computational chemistry methods is presented in this work to try and resolve the thermochemical values.

Enthalpies of formation of trans- and cis-HONO and HNO_2 are determined using a variety of model chemistries including DFT methods. The calculations are combined with work reactions to isomerization (Table IV), atomization reactions (Table V), isodesmic work reactions involving closed-shell species (Table VI), and work reactions with open-shell-species (Table VII).

Heats of formation for trans-HNOO, cis-HNOO, trans-HOON, cis-HOON, and HcyNOO pyramidal high-energetic isomers are also evaluated using an atomization procedure and by use of work reactions.

THEORETICAL CONSIDERATIONS AND COMPUTATIONAL METHODS

Geometry optimizations and other calculations are performed using DFT and the ab initio based composite methods CBS-QB3 [59], CBS-APNO [60], and G3 [61], as implemented in the Gaussian 03 suite of programs [62]. Transition state structures (TS) were confirmed to have one imaginary frequency along the reaction coordinate. Connectivity of stationary points has been checked using intrinsic reaction coordinate (IRC) analysis [63].

CBS-APNO: The complete basis set extrapolation method of Petersson and coworkers using an atomic pair natural orbital basis set (CBS-APNO) [60] is the highest level method we used. The calculation includes a HF/6–311G(d,p) geometry optimization to obtain the enthalpy and free-energy corrections, with final

Table IV Comparison of Heats of Formation ($\Delta H^{\circ}_{f\,298}$, kcal mol^{-1}) for Simple H/N/O Systems Using Atomization Energy Reaction[a] vs. Experimental Data

Species	CBS-QB3	CBS-APNO	G3	AvgCM[b]	Experimental
NO	20.76	22.04	21.80	21.53	21.58[c], 21.76[d]
NO$_2$	6.02	6.39	8.13	6.85	7.91[c], 8.12[d]
HNO	24.60	26.11	26.41	25.71	25.6[e]
HONO-*trans*	−20.17	−18.73	−17.92	−18.94	−18.84[f], −18.87[g]
HONO-*cis*	−19.81	−18.26	−17.35	−18.47	−18.3[h], −18.34[f], −18.51[g]
HNO^2	−12.30	−10.54	−9.98	−10.94	...
HNOO-*trans*	56.99	58.33	60.88	58.73	...
HNOO-*cis*	54.37	55.45	59.47	56.43	...
HOON-*trans*	24.68	...[i]	34.89	...[j]	...
HOON-*cis*	26.59	...[I]	30.35	...[j]	...
HcyNOO	61.99	64.82	66.00	64.27	...
HONO$_2$	−35.21	−32.99	−31.70	−33.30	−32.10[c]

[a] In kcal mol^{-1}.

[b] AvgCM—evaluated average of composite models.

[c] From *NIST Webbook* [46].

[d] From Ruscic et al. [76].

[e] From Anderson [71].

[f] From Chase [48].

[g] From Gurvich et al. [49].

[h] Originally: HNO$_2$-*cis*, Benson [50].

[i] No convergence in quadratic configuration interaction localization.

[j] Because of the large differences in energy of two composite methods, the average value was not used.

geometry reoptimized at QCISD/6–311G(d,p) level of theory. This QCISD geometry is then used in single-point calculations using the QCISD(T), MP2(Full), HF, and MP2 methods. The CBS-APNO extrapolation in the last steps computes the final energies. The unique feature of the CBS family of model chemistries is the incorporation of an algorithm for the extrapolation of second-order pair energies calculated to the infinite-order pair energies at the complete basis set limit.

CBS-QB3: This is a relatively low-cost complete basis set method. Geometries and frequencies are calculated at B3LYP/6–311G(2d,d,p) level. This basis set denoted originally as the CBSB7 basis includes 2d functions on the second row elements, d-polarization function on the first row, and additional p-polarization function on hydrogen atoms. This p-polarization is indicated [59] to result in better transition state structure for hydrogen transfer reactions. Two additional calculations are used to approximate higher order of contributions MP4(SDQ)/6–31+G(d(f),p) and CCSD(T)/6–31+G†. In place of quadratic configuration interaction QCISD(T) used in CBS-APNO, the coupled cluster singles and doubles with perturbative triples CCSD(T) are used. The CCSD(T) is considered to improve accuracy over the QCISD(T) method, especially for spin-contaminated radicals [59,64]. The 6–31G† basis is a modification of the 6–31G(d,p) basis obtained combining the 6–31G *sp* functions with the 6–311G(d,p)

polarization exponents. There are also correction for spin contamination (proportional to $\langle S^2 \rangle$) and size-consistent higher order empirical correction. The numerical coefficients were determined from experiment using dissociation energies of the 55 molecule G2 test set and eight selected systems including NO for which an electron affinity parameter is used.

G3: This method [61] falls between the two CBS methods (above) in terms of computational cost. The G3 protocol begins with a HF/6–31G(d) geometry optimization and a frequency calculation, with the frequencies scaled by 0.8929. The third step is a MP2(Full)/6–311G(d) geometry optimization. The improved MP2 geometry then used for a series of single-point calculations at the QCISD(T,E4T)/6–31G(d), MP4/6–31+G(d), MP4/6–31G(2df,p), and MP2(Full)/G3large levels. Corrections are applied to approximate the contributions of diffuse and higher polarization functions at the MP4 level and a correction for correlation effects beyond MP4 using quadratic configuration interaction. The G3 method also contains an empirical correction step to account for core-valence correlation and for unpaired valence electrons. Entropic and thermal contributions in G3 are based on the HF/6–31G(d) structure and frequencies.

Appendix A1 provides details of the atomization reaction to 0 K ± thermal correction method (conventional method) used to calculate enthalpy of formation

Table V Composite Method Results on Heats of Formation of Nitrous Acid Isomers Using Conversion to *trans*-HONO Work Reactions[a] and Stability of Isomers ($\Delta H_i^{298} = E_i - E_E$, Relative to (*trans*-) E-HONO)

	ΔH_{f298}° (kcal mol^{-1})					ΔH_i^{298} (kcal mol^{-1})			
Species	CBS-QB3	CBS-APNO	G3	AvgCM[b]	Literature	CBS-QB3	CBS-APNO	G3	Literature
HONO-*trans*	ref	ref	ref	ref	**−18.87**[c]	0.00	0.00	0.00	0.00
HONO-*cis*	−18.49	−18.37	−18.27	−18.38	**−18.34**[d]	0.35	0.47	0.57	**0.40**[h] **0.37**[i] −0.62 to −1.44[j] 0.5 to 0.8[k] 0.44[l] −1.43[e]
HNO$_2$	−10.98	−10.65	−10.90	−10.84	−14.15[e,f]	7.86	8.19	7.94	15.77[m] 8.2[n] 3.53[e] 8.5[k]
HOON-*trans*	26.01	…[g]	33.97	…	39.34[e]	44.85	…[g]	52.81	57.7[e] 67.6[o]
HOON-*cis*	27.92	…[g]	29.43	…	46.32[e]	46.76	…[g]	48.27	64.7[e] 73.3[o]
HNOO-*trans*	58.31	58.22	59.96	58.83	57.07[e]	77.15	77.06	78.98	75.4[e]
HNOO-*cis*	55.70	55.34	58.55	56.53	54.56[e]	74.54	74.18	77.39	62.9[e]
HcyNOO	63.32	64.71	65.08	64.37	65.01[e]	82.16	83.55	83.92	83.35[e] 81.1[p]

[a] Experimental data are given in bold.
[b] AvgCM—average of composite methods.
[c] Benchmark experiment [49].
[d] From Benson [50].
[e] BAC-MP4 [37].
[f] From Kee et al. [58a] and Bromly et al. [58b].
[g] No convergence at QC1 localization.
[h] Using IR intensities [28].
[i] Using microwave intensities [29].
[j] From Nakamura et al. [40a] using up to MP4/D95** level.
[k] From Jursic [19b], at 0 K within the CBSQ method.
[l] The reported best result of [23] using CCSD(T)/6–311++G(2df,2p).
[m] From Takane and Fueno [39], within the MRD–CI/6–31G(d,p) using ZPE correction with SCF vibrations.
[n] From Nakamura et al. [40a], relative to cis-HONO at CASSCF/4-31G(d).
[o] From Nakamura et al. [40a], relative to cis-HONO at MP3/6-31G(d) level relative to cis-HONO.
[p] From Nakamura et al. [40a], at MP3/6-31G(d) level relative to cis-HONO.

Table VI Calculated Heats of Formation- ΔH^{o}_{f298} (kcal mol^{-1}) of HONO Isomers Using Work Reactions (2)–(6) with Closed -Shell Species (HNO, HONO$_2$, CH$_3$ONO, and CH$_3$NO$_2$)

Reaction # Species	(2) HNO$_2$	(3)[a] HNO$_2$	(4) HNO$_2$	(5) HONO-*trans*	(6)[a] HONO-*cis*
CBS-QB3	−9.52	−10.59	−10.69	−18.59	−17.53
CBS-APNO	−10.06	−10.53	−10.54	−18.34	−18.28
G3	−10.28	−10.49	−10.39	−18.24	−18.14
AvgCM	−9.95	−10.85	−10.54	−18.49	−17.48
Experimental				−18.87[b]	−18.34[c]

[a] The cis form is the most stable isomer of CH$_3$ONO and is used for evaluation—see text.

[b] From Gurvich et al. [49].

[c] From Chase [48].

as well as an alternate scheme (Appendix A2) for calculation of $\Delta H^{o}_{f(298\ K)}$ using atomization reaction direct to 298 K.

RESULTS AND DISCUSSION

Literature and Reference Species Data

A listing of thermochemical data on the selected NO$_x$ compounds as well as data on molecules we use as reference in the work reactions is provided in Table I.

Structures and Vibration Frequencies

Geometries and energies (in atomic units) are listed in Table II for *cis*- and *trans*- HONO and HNO$_2$.

The highest level of theory for geometry optimization employed here is CBS-APNO, which uses QCISD/6–311G(d,p) [60], whereas G3 uses MP2(Full)/6–31G(d). Comparison of geometry parameters shows that the DFT method calculates the structure parameters quite well, which is in agreement with data from the Petersson research group [59].

Harmonic frequencies and moments of inertia from the different calculation levels are presented in Table III along with experimental data [28a,b]; these

frequency values are scaled by the factors noted in the table caption for calculation of ZPVE and thermal energy. Overall, there is acceptable agreement with experimental values, and the QCISD(T)6–311+G(d) calculations [34] show the better agreement with experiment.

We note that among multilevel calculation methods, only the CBS-QB3 uses the same method (B3LYP/6–311(2d,d,p)) for both geometry and frequencies, with a zero-point adjustment factor of 0.99. This is also important for localization of transition states and internal reaction coordinates [59] because the frequency data matches the structure. Vibration frequencies within the G3 and CBS-APNO methods are calculated on SCF basis, HF/6–31G(d), and HF/6–311G(d), respectively, scaled by factor 0.8929 in G3 and 0.99 in APNO.

Standard Enthalpies of Formation

Heats of formation for the HONO-isomers, ΔH^{o}_{f} (298 K), have been obtained using four different reaction analyses (i) atomization, (ii) isomerization, (iii) work reaction with stable species, and (iv) work reactions using radicals. Comparison of the enthalpy data on species from these four different analysis methods is quite interesting.

Table VII Calculated Heats of Formation (ΔH^{o}_{f298}, kcal mol^{-1}) on Isomers of Nitrous Acid Using Work Reactions (7–11) Containing Open-Shell Species

| Work Reaction Species	(7) HONO-*trans*	(8) HONO-*cis*	(9) HNO$_2$	(10) HNO$_2$	(11) HNO$_2$
CBS-QB3	−18.16	−17.80	−10.20	−9.70	−9.91
CBS-APNO	−19.85	−19.38	−9.05	−9.17	−8.73
G3	−18.36	−17.78	−10.76	−10.16	−10.84
AvgCM[a]	−18.67	−18.32	−10.00	−9.68	−9.83
Experiment	−18.87[b]	−18.34[b]	—	—	

[a] Evaluated average of composite model results.

[b] From Gurvich et al. [49].

Heats of Formation by Atomization Energies. The most common method to determine enthalpy uses atomization reactions (vide supra), where enthalpies of formation at 298.15 K are computed from the reaction and the experimental enthalpies for constituent atoms. We utilize atom enthalpies at 298 K recommended by NIST as listed in Table I and Appendix A. A second set of atom enthalpies is at 0 K [67,68] with the temperature corrections ($\Delta H^{\mathrm{T}} = H^{298} - H^0$) for atoms of elements in their standard states. The thermal energy correction values in this 2nd set are 0.25, 1.01, 1.04, and 1.04 kcal mol^{-1}, for C, H, O, and N atoms, respectively. Table IV compares results of our model calculations of $\Delta H_{\mathrm{f}}^{\mathrm{o}}$ (298 K) for HONO isomers as well as those for NO, NO$_2$, HNO, and HONO$_2$ as reference molecules.

The average atomization enthalpy value from the three composite methods (AvCM) for NO, HNO, HONO-, *cis*, and HONO-*trans* is in excellent agreement (within 0.5 kcal mol^{-1} or less) with experimental data as illustrated in Table IV. Deviations among the multilevel methods are not systematic when compared to experimental data. CBS-QB3 and G3 overestimate and underestimate stability of *trans*-HONO, respectively. CBS-APNO predicts the $\Delta H_{\mathrm{f}}^{\mathrm{o}}$ (298 K) almost quantitatively. The same trend is observed for HNO. The CBS-APNO underpredicts the recommended experimental values for NO$_2$ by 1.27 kcal mol^{-1}. This deviation in the NO$_2$ enthalpy is discussed further below. For the major species in Table IV, CBS-QB3 estimates enthalpies of formation that are 1–2.5 kcal mol^{-1} lower than the selected values for NO, HNO, HONO, HNO$_2$, and HONO$_2$. G3 values are higher than selected values by 0.4–1 kcal mol^{-1} with the exception of HNO.

One important target in this study is the enthalpy for the HNO$_2$ structure; we find the $\Delta H_{\mathrm{f}}^{\mathrm{o}}$ (298 K) from the three composite methods using atomization reaction analysis is near -10.94 kcal mol^{-1}, which is 8 kcal mol^{-1} higher than *trans*-HONO.

Heats of Formation from Isomerization (Interconversion) Reaction Analysis. From the results of our calculation and evaluation of the literature, we identify and use the experimental value for the heat of formation of *trans*-HONO (-18.84 kcal mol^{-1}) as a benchmark. The $\Delta H_{\mathrm{f}}^{\mathrm{o}}$ (298 K) for the other isomers of HONO can then be determined using isomerization work reaction and the known $\Delta_{\mathrm{f}} H_{298}^{\mathrm{o}}$ of HONO-*trans* (Table V):

$$\text{Isomer of } \mathrm{HNO_2} \rightarrow \textit{trans}\text{-HONO} \qquad (1)$$
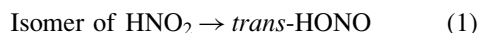
This analysis allows a cancellation of errors across the reaction and results in dramatically increased consistency across the calculation methods as can be observed in Table V. The isomerization analysis also provides several ways to assess the calculation errors: (i) analysis of the relative enthalpy values, (ii) analysis of the difference, and (iii) direction of change from between isomer enthalpies. The comparison can also suggest the degree that a given bond type has in determining computational errors of particular isoelectronic system.

In one view, the values derived from calculations of energy difference in this isoelectronic system might be considered the most internally consistent, because of the likely cancellation of errors occurring on each side of the equation. A different evaluation suggests that errors from use of isomerization analysis for enthalpy may result from nonconservation of bond energies. For example, it is reported that some nitrite and nitro systems have diradical character and require a multiconfiguration approach. One may also consider the hydroperoxynitrene molecule (HOON) as a near Van der Waals complex between OH and NO because of the large interatomic separation of oxygen atoms (vide supra; Table II). A second case exists in the transition state of HNO$_2$ isomerization to *trans*-HONO, which when localized using CASSCF procedure was described as an interacting system of proton and the nitrite anion, rather than as a pair of two fragment radicals [39].

Calculation results from isomerization reaction analysis and literature data are presented in Table V, where there is excellent agreement between results of composite methods for HONO and HNO$_2$ isomers in addition to good agreement between HNOO and HcyNOO. The enthalpy values for the three calculation methods (QB3, APNO, G3) are within ± 0.15 kcal mol^{-1} and all predict the cis isomer at a slightly higher energy (0.46) relative to *trans*-HONO, with HNO$_2$ being 8 kcal mol^{-1} higher in enthalpy than *trans*-HONO. The 0.4–0.5 kcal mol^{-1} higher $\Delta H_{\mathrm{f\,298}}^{\mathrm{o}}$ for the *cis*-HONO isomer is in full accord with experimental data on cis–trans isomer preference [29,30]. Significant variation between the composite method calculations for HOON is obvious, with deviations to 17 kcal mol^{-1}.
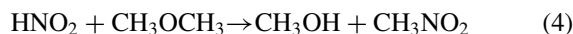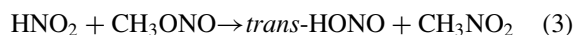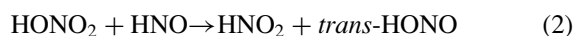
The average enthalpy of formation from the higher level composite methods for HNO$_2$ is -10.84 kcal mol^{-1}, and this is close to the value computed from the atomization reactions of -10.94 kcal mol^{-1}. We recommend the -10.9 ± 0.05 value for $\Delta H_{\mathrm{f}}^{\mathrm{o}}$ (298 K) of HNO$_2$.

Estimation of Heats of Formation Using Conventional Work Reactions. Application of isodesmic reaction calculations often yields heat of formation values that are in close agreement with available
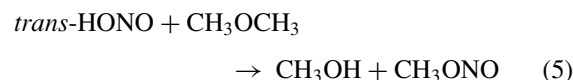
experimental data. Use of this work reaction method requires that enthalpies of all species but one in the reaction be taken either from experiment, from the literature, or reliable calculations. The improved accuracy from use of isodesmic reactions, in which the number of each type of bonds is preserved on both sides, results from the cancellation of systematic errors.

We calculate ΔH_f^o (298 K) for HONO isomers and study the dependence of ΔH_f^o (298 K) on type of species viz. bond types and methods employed in isodesmic reactions to estimate possible errors and additivity of such uncertainties. Tables VI and VII compare our computed ΔH_f^o (298 K) results on heat of formations of HONO isomers using the three composite theories with work reactions that involve closed-shell molecules (Table VI), and work reactions with open-shell species (Table VII).

Experimental data for reference species used in the work reactions are reported in Table I. ΔH_f^o (298 K) for HNO_2 is determined using the following reactions:

$$HONO_2 + HNO \rightarrow HNO_2 + trans\text{-}HONO \qquad (2)$$

$$HNO_2 + CH_3ONO \rightarrow trans\text{-}HONO + CH_3NO_2 \quad (3)$$

$$HNO_2 + CH_3OCH_3 \rightarrow CH_3OH + CH_3NO_2 \qquad (4)$$

Reactions (5) and (6) are employed for computation of $\Delta H_{f(298\ K)}^o$ for $trans$-HONO and cis-HONO:

$$trans\text{-}HONO + CH_3OCH_3$$
$$\rightarrow CH_3OH + CH_3ONO \qquad (5)$$

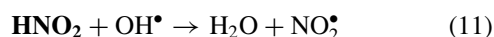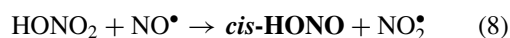$$HONO_2 + HNO \rightarrow cis\text{-}HONO + trans\text{-}HONO \qquad (6)$$

Reactions (3)–(5) use a methyl group to replace a hydrogen atom, whereas reactions (1) and (6) use only HNO_x species.

Precision and accuracy across the three calculation methods and five work reactions are illustrated in Table VI for CBS-QB3, APNO, and G3 calculations for HNO_2 and for HONO isomers. The average value for cis-HONO is -17.48 kcal mol^{-1} (reaction (6)) and -18.49 for the $trans$-HONO (reaction (5)). CBS-QB3, CBS-APNO, and G3 calculations result in an average $\Delta H_{f(298\ K)}^o$ for HNO_2 of -9.95 (reaction (2)), -10.85 (reaction (3)), and -10.54 (reaction (4)), respectively with deviations less than 0.5 kcal mol^{-1}. Reaction (2) conserves the number of bonds and bond order between each pair of atom types. The results of the work reaction analysis are in good agreement with the isomerization and atomization reaction analysis.

The results for $trans$-HONO and HNO_2 are similar in all three composite methods, and there is good agreement with the values from the isomerization and atomization reaction analysis.

Estimation of the Heats of Formation Using Work Reactions Including Open-Shell Species. It is expected that the use of all closed-shell molecules in the work reactions (above) will yield better results than the use of open-shell species. However, there is value in evaluating open-shell reactions and sometimes it is important to use open-shell species to conserve atom environments.

The work reactions (7) and (8) are used to calculate the enthalpy of formation for $trans$- and cis-HONO, whereas reactions (9)–(11) are used to calculate enthalpy of the HNO_2 structure, as denoted in bold below. We further note that the electronic environment in the $NO_2^\bullet$ radical is not similar to that in $NO^\bullet$, $HC^\bullet{=}O$, or OH.

$$HONO_2 + NO^\bullet \rightarrow \textbf{\textit{trans}-HONO} + NO_2^\bullet \quad (7)$$

$$HONO_2 + NO^\bullet \rightarrow \textbf{\textit{cis}-HONO} + NO_2^\bullet \qquad (8)$$

$$HNO + NO_2^\bullet \rightarrow \textbf{HNO}_2 + NO^\bullet \qquad (9)$$

$$\textbf{HNO}_2 + HC^\bullet{=}O \rightarrow NO_2^\bullet + CH_2O \qquad (10)$$

$$\textbf{HNO}_2 + OH^\bullet \rightarrow H_2O + NO_2^\bullet \qquad (11)$$

Data for the two CBS and the G3 composite calculations are listed in Table VII.

The enthalpies from the CBS-QB3 and G3 methods for the $trans$- and cis-HONO are in agreement with all the previous calculations with the trans (cis) isomers at -18.16 (-17.80) and -18.36 (-17.78) kcal mol^{-1}, respectively. The higher level APNO calculation predicts enthalpies of -19.85 and -19.38, some 1.0 kcal mol^{-1} low relative to experiment (-18.84), and previous calculation results (average composite value -18.67), including data from CBS-APNO on heats of atomization (-18.73). Analysis of this data and the data in the Table IV on heats of atomization show that the reason for low enthalpy of formation in HONO from APNO calculation on work reactions (7) and (8) is the underprediction on the enthalpy of NO_2 by CBS-APNO, 6.39 versus the value used in the work reaction 8.12 kcal mol^{-1}. (Please see data in Table IV and discussion on this table above.) If one adjusts the ΔH_f^o (298 K) of NO_2 in the work reaction to that of the CBS-APNO value ($+1.27$), one obtains -18.55 for CBS-APNO on $trans$-HONO, which is only 0.18 kcal mol^{-1} different from the CBS-APNO value from atomization reaction.

Analysis of the HNO_2 data in Table VII also shows that the highest level calculation, CBS-APNO with the work reactions (9)–(11) predicts the ΔH_f^o (298) of HNO_2 to be too high by slightly more that 1 kcal mol^{-1} (average) relative to the CBS-QB3 and G3. Correcting

Table VIII   Ideal Gas Phase Thermodynamic Properties of HONO Isomers[a]

Species	ΔH^o_{f298}	S^o_{298}	$C_P(300)$	$C_P(400)$	$C_P(500)$	$C_P(600)$	$C_P(800)$	$C_P(1000)$	$C_P(1500)$
HONO-*trans*	−18.9	57.89	10.72	12.13	13.26	14.16	15.46	16.36	17.74
HNO$_2$	−10.9	55.56	9.19	10.44	11.71	12.84	14.60	15.84	17.62
HONO-*cis*	−18.4	57.64	10.31	11.77	12.98	13.95	15.36	16.33	17.77

[a] Thermodynamic properties are referred to a standard state of an ideal gas at 1 atm. Enthalpies are in kcal mol^{-1}; entropy and heat capacities are in cal mol^{-1} K^{-1}.

the average value from the APNO calculation by subtracting 1.27 for the APNO adjustment to NO$_2$, which occurs in each of the work reactions (9)–(11), results in a value of −10.25 for the HNO$_2$ isomer. Cancellation of error does not appear to be occurring in these five reactions for the CBS-APNO method.

Entropy, S°(298 K), and Heat Capacities, C$_p^o$ (T), of HONO Isomers

Entropy and heat capacity values from vibration, translation, and rotation contributions are calculated using the rigid-rotor-harmonic-oscillator approximation. SMCPS code (Statistical Mechanics for Heat Capacity and Entropy) [65] is used for evaluations, based on scaled vibration frequencies, and moments of inertia from the optimized by B3LYP/6–31G(d,p) structures in Table III. $\Delta H^o_{f(298\,K)}$, $S_{(298)}$, and heat capacity data (to 1500 K) are listed in Table VIII.

The torsion frequency used for contribution to $S^o(298)$ and $C_p^o(T)$ is from the internal rotor and not a separate internal rotor analysis, because of the high barrier of *cis*- to *trans*-HONO isomerization. The calculated barrier is 12.89, 11.93, 9.90, 10.04, and 10.16 kcal mol^{-1} at B3LYP/6–31G(d,p), B3LYP/6–311G(2d,d,p), CBS-QB3, G3, and CBS-APNO meth-

ods, respectively. The composite methods show very good agreement with the experimental [45] value of 10.16 kcal mol^{-1} for this barrier.

Bond Dissociation Enthalpies

Table IX illustrates the results from the calculations on the homolytic bond cleavage energy data for HONO and HNO$_2$.

$$\textit{trans-}HONO, \textit{cis-}HONO \rightarrow OH + NO$$

$$HNO_2 \rightarrow H + NO_2$$
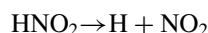
Bond dissociation enthalpies of 49.2 kcal mol^{-1} for the HO—NO bond can be estimated from the NIST data tables [46] by considering the dissociation of *trans*-HONO to OH + NO. Note that this value was suggested for use as an accuracy test in basis set studies by Bauerfeldt et al. [24].

Using reevaluated enthalpy of formation for hydroxyl radical, ΔH^o_f (298 K) equal to 8.93 kcal mol^{-1} [76], and the recommended value of −18.84 kcal mol^{-1} for *trans*-HONO [48], one can derive 49.53 kcal mol^{-1}.

A direct measurement of the homolytic BDE of *trans*-HONO by double-resonance overtone

Table IX   Comparison of Calculated and Literature Bond Dissociation Energies (kcal mol^{-1})

	HO—NO-*trans*	HO—NO-*cis*	H—ONO-*trans*	H—ONO-*cis*	H—NO$_2$
CBS-QB3	49.76	49.41	78.29	77.93	70.43
CBS-APNO	49.86	49.38	77.23	76.75	69.04
G3	48.14	47.57	78.16	77.58	70.20
AvgCM[a]	49.25	48.78	77.89	77.42	69.89
Experiment	49.24[a]	49.20[a,c]	78.35[a]	78.31[a,c]	—
	49.56[b]	49.03[b,c]	78.56[b]	78.52[b,c]	—
	48.01[d]				
	49.58 [e]				
	48.00[f]				

[a] Using NIST dataset including the value of −18.34 kcal mol^{-1} presented for *trans*-HONO [46].
[b] Using novel data of Ruscic et al. [76] = 21.76 + 8.93 − (−18.87).
[c] Using value of −18.34 kcal mol^{-1} for *cis*-HONO [48].
[d] DROPS spectroscopic data [40].
[e,f] Kinetic data on decomposition of HONO: recommended [11a] and experimental [l1b] data, respectively.
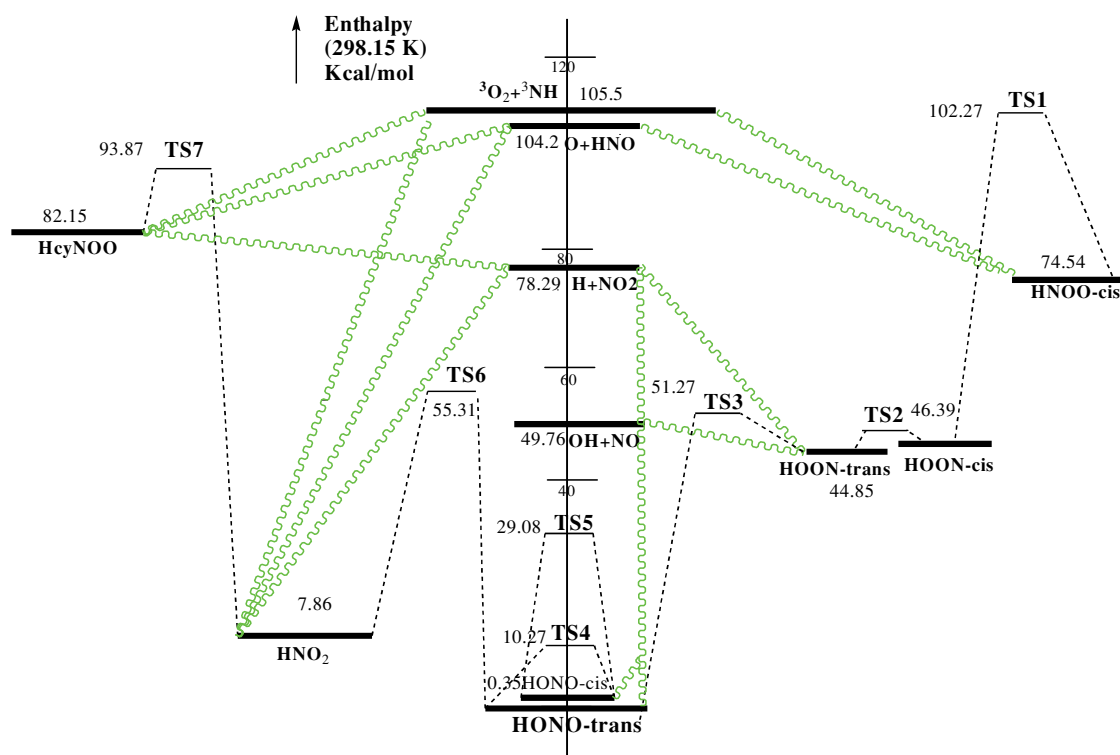
Figure 2 Potential energy diagram: formation and decomposition of HONO-isomers calculated at the CBS-QB3 composite level (Table X). TS (i) denote the transition states of interconversion processes: TS1—1,3 hydrogen shift; TS2—cis–trans isomerization of HOON; TS3—conversion of HOON to HONO; TS4—*cis* to *trans* isomerization in HONO; TS5—hydrogen "hopping" H-shift oxygen to oxygen in *cis*-HONO; TS6—1,2 hydrogen shift leading to the conversion of HONO to HNO₂; TS7—cyclization of HNO₂ *via* pyramidal transition state. Toothed (saw-like) lines in green indicate on direct formation and decomposition pathways. [Color figure can be viewed in the online issue, which is available at www.interscience.wiley.com.]

photofragment spectroscopy (DROPS) [44] gave 48.01 kcal mol⁻¹. There is also a value of 49.58 kcal mol⁻¹ based on a comprehensive evaluation of literature kinetic data on the decomposition of HONO by Tsang et al. [11].

The 49.25 kcal mol⁻¹ average value from the three composite methods is in excellent agreement with the NIST-recommended data, but this average is a result of two CBS values of −49.76 and −49.86 and the G3 value of −48.14, which bracket the NIST value. The G3 model chemistry value of 48.14 kcal mol⁻¹ agrees well with the DROPS experiment.

The average values from the composite methods in Table IX results in the 77.9 for the H—ONO bond in the trans isomer, where the isonitrous acid, H—NO₂, bond is weaker at 69.9 kcal mol⁻¹.

Potential Energy Surface of H/N/O₂ System

The formation, decomposition, and interconversion paths are presented in the form of an enthalpy diagram for HONO isomers using the CBS-QB3 composite method in Figs. 2 and 3 and Table X.

The CBS-QB3 calculations for the HcyNOO, HOON, HNOO, and TST species in the energy diagram are chosen for several reasons. CBS-APNO failed to predict a stable HOON structure in configuration interaction localization step using the QCISD(T)/6–31g(d,p) calculation. G3 also has some deficiencies in estimation of TS enthalpies: G3 predicts energies for HOON that are 4–5 kcal mol⁻¹ higher, placing the HOON isomers at the same energy as the NO + OH dissociation products. The frequencies and structure in G3 for the conversion of HNO₂ to cyclic imine peroxide along the pyramidal mode (TS7, Fig. 2) are based on a G3//HF/6–31G(d) structure. This geometry is, however, changed (shifted) to the TS of decomposition to HNO + O(³P) in the next step, the MP2/6–31G(d,p) optimization of the (TS) structure. The enthalpy of this TS would not be correct because it is based on the ZPE and total electronic energies of different (TS) structures. The CBS-QB3 uses the same approximation for both frequency and geometry calculations, viz. the B3LYP hybrid functional and 6–311(2d,d,p) basis set. This is an important advantage of this composite method at least for systems under consideration.
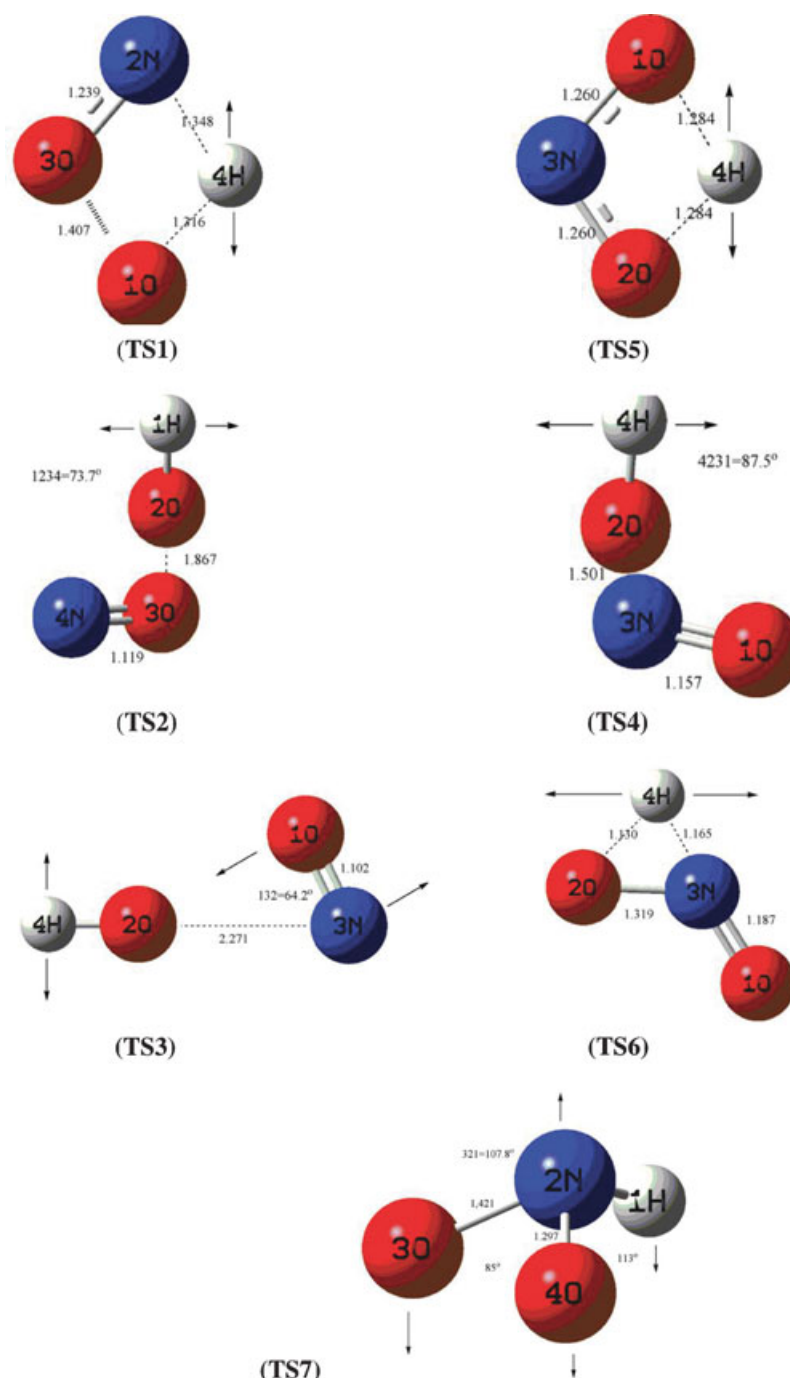
Figure 3 Transition states of HONO transformations: Top: 1,3-shifts (intramolecular) of hydrogen atom, TS1—conversion of HNOO to HOON, TS5—*cis*-HONO molecule into itself (hydrogen atom hopping). Middle: cis to trans isomerization of HOON (TS2) and in HONO (TS4); conversions of HOON-*trans* to HONO-*trans* (TS3) and HONO-*trans* to HNO$_2$ (TS6). Bottom: Cyclization of HNO$_2$ via pyramidal transition state (TS7). [Color figure can be viewed in the online issue, which is available at www.interscience.wiley.com.]

Formation of HNOO in high-energy combustion media presumably takes place via the chemically activated reaction of molecular oxygen plus triplet NH with well depth of 31 kcal mol^{-1} and the reaction of O(^{3}P) + HNO with well depth of 29.7 kcal mol^{-1}. A

detailed discussion of previous data on these processes can be found in Chapter 2 of the combustion chemistry monograph [16].

The conversion of the HNOO to HOON proceeds via a 1,3-hydrogen shift with an activation barrier of

Table X Enthalpies of Reactants, Products, and Stationary Points on PES of HONO Isomers and Imaginary Frequencies of TS Structures, CBS-QB3//B3LYP/6–311G(2d,d,p)

System	H_{298} (au)	$v_i^{\#}$ (cm^{-1})
HONO-*trans*	−205.470808	
HONO-*cis*	−205.470243	
HNO$_2$	−205.45828	
HOON-*trans*	−205.399335	
HOON-*cis*	−205.396294	
HNOO-*cis*	−205.352021	
HNOO-*trans*	−205.347856	
HcyNOO	−205.339883	
TS1	−205.307825	i2002.82
TS2	−205.396886	i287.12
TS3	−205.389106	i465.71
TS4	−205.454439	i669.18
TS5	−205.424472	i1920.61
TS6	−205.382662	i2096.31
TS7	−205.321211	i1398.08
^{3}O2 + ^{3}NH	−205.302594	
HNO + O	−205.304758	
OH + NO	−205.391507	
H + NO$_2$	−205.346048	

27.7 kcal mol^{-1} (TS1). The cis-conformer of hydroperoxynitrene, *cis*-HOON, in turn dissociates to OH + NO or transforms to *trans*-HONO (TS3, ΔH_a = 6.4 kcal mol^{-1}) after a rotation about O—O axis via TS2. The reverse reaction HONO-*trans* to HOON must overcome a barrier of 51.3 kcal mol^{-1}.

The two combination reactions above, NH + O$_2$ and HNO + O, can also lead to the formation of chemically activated HNO$_2^*$ with much deeper well depths than in formation of HNOO above: 97.7 and 96.3 kcal mol^{-1}, respectively. Both of these HNO$_2^*$ formation reactions will lead to dissociation into H + NO$_2$ at atmospheric and lower pressures.

The calculated barrier for conversion of *trans*-HONO to HNO$_2$ via a 1,3-hydrogen shift (TS6) is 55.3 kcal mol^{-1}, where ΔH_{rxn} is only 8 kcal mol^{-1}. This barrier is in good agreement with data of Nguyen et al. (55.8 kcal mol^{-1}) [23] calculated at the CCSD(T)/6–311++G(3df,2p)//CCSD(T)/6–31G(d,p) level of theory. The *trans*-HONO to HNO$_2$ barrier is 4 kcal mol−1 higher than conversion of *trans*-HONO to *trans*-HOON (TS3), where ΔH_{rxn} is 45 kcal mol^{-1}. The activation energy for the reverse reaction, HNO$_2$ isomerization to HONO, is 47.45 kcal mol^{-1}.

The stability of HNO$_2$ is somewhat higher than that of HONO. The HONO will undergo unimolecular dissociation to NO + OH with a bond energy of only 49 kcal mol^{-1} and a high pre-exponential factor ∼ 6.E14. The HNO$_2$ will isomerize with a similar barrier (48 kcal mol^{-1}), but with a pre-exponential factor (∼5.E13) which is lower than that for HO—NO bond cleavage.

The elementary, unimolecular rate constant for the HNO$_2$ reaction to *trans*-HONO, calculated using canonical transition state theory (Thermkin code [77]) was fitted to a three-parameter (A, n, Ea) modified Arrhenius equation over a temperature range of 298–1500 K

$$k(\mathrm{HNO_2 \to HONO}) = 1.70 \times 10^{11} \times T^{0.93}$$

$$\exp(-47{,}667\ \mathrm{cal}/RT)\mathrm{sec}^{-1}$$

This rate constant is not adjusted for pressure fall off.

The frequency factor of HONO → OH + NO dissociation reaction is $A = 6.13 \times 10^{14}$ s^{-1} obtained by Nguyen et al. [23] using canonical variational transition state theory at B3LYP/6–31G(d,p) level of theory and a Morse potential fit for interatomic distances 1.5–2.8 Å.

The barrier of 9.91 kcal mol^{-1} calculated for cis to trans isomerization of HONO (TS4) is in good agreement with experimental data [42,43] of 8.7–11.5 kcal mol^{-1} as discussed above.

Table XI Activation Energies (ΔH_a, kcal mol^{-1}) and Imaginary Frequencies (v_i, cm^{-1}; in parentheses) for *trans*-HONO Isomerization Transition States vs. Calculation Method

	cis- to *trans*-HONO[a]	*trans*-HONO to HOON[b]	*trans*-HONO to HNO$_2^c$
B3LYP/6–31G(d,p)	12.89 (i685.3)	60.29 (i484.3)	54.97 (i2075.8)
B3LYP/6–311G(2d,d,p)	11.93 (i669.2)	56.09 (i465.7)	55.53 (i2096.3)
CBS-QB3//B3LYP/6–311G(2d,d,p)	9.91 (i669.2)	51.27 (i465.7)	55.31 (i2096.3)
CBS-APNO//HF/6–311G(d,p)	10.16 (i616.7)	−[d](i375.0)	54.59 (i2648.4)
G3//HF/6–31G(d)	10.04 (i617.7)	46.91[e] (i445.2)	55.09 (i2714.7)

[a] Corresponds to TS4 on PES—Fig. 2.

[b] TS3.

[c] TS6.

[d] No convergence at QCI localization.

Transition state TS5 corresponds to the intramolecular migration ("hopping") of hydrogen atom from oxygen to oxygen in HONO-*cis* with conversion into the same isomer; the TS5 has C_{2v} symmetry. This H atom migration barrier is 29.1 kcal mol^{-1} at the CBS-QB3 level, some 20 kcal mol^{-1} lower than HONO dissociation to OH + NO. This reaction path may be an explanation for the observation of rapid oxygen atom isotope exchange between ^{18}OH and N^{16}O in flow tube experiments [78], which used magnetic resonance detection of ^{18}OH and ^{16}OH radicals. Hydrogen atom hopping in HONO has also been observed theoretically in molecular dynamic simulations using a potential energy surface constructed from the semiempirical PM3 method [1c].

CBS-QB3 predicts a barrier of 86 kcal mol^{-1} for cyclization of HNO$_2$ via pyramidal transition state TS7 to HcyNOO with an activation enthalpy of 11.72 kcal mol^{-1} for the reverse reaction as shown in Fig. 2.

Data in Table XI illustrate activation parameters for isomerization reactions of *trans*-HONO from the different methods; they also show very good consistency for calculation of the barrier.

Some discrepancy exists between the DFT- and HF-calculated harmonic frequencies for the transition state structure of the HONO to HNO$_2$ conversion, but the bond distances in the transition state do not differ substantially. Properties of the weakly bound HOON do not show consistency between the calculation methods.

Triplet State Energies and Some Reactions on the Triplet Surface, Not Shown in Fig. 2
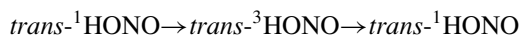
The triplet state of HONO isomers is some of mechanistic interest. The HNOO^T is reported [16,37] to be one of the intermediates in high-energy combustion processes. It would be interesting to study reaction channels of HONO transformations in this lower exited state PES.

We could not localize a stable triplet state for the cis isomer of HONO at CBS-QB3 (viz. at DFT optimization) level. The *cis*-HONO^T isomer (unexpectedly) transforms to the trans isomer (rotation of the OH-group about the N−O bond) upon full geometry relaxation. The cis isomer appears not to be a local minimum on the triplet PES of HONO at this hybrid DFT B3LYP/6–311G(2d,d,p) level of calculation for structure. The phenomenon is supported by similar results from higher level QCISD/6–311+G(d,p) calculations as well as by the analogous results in study of CH$_3$ONO^T isomers.

Calculations at the CBS-QB3 level predict the electronic transitions from singlet states of cis and trans isomers of HONO to the triplet state of HONO-

trans require energies for ΔE (*trans*-HONO^S–*trans*-HONO^T) of 56.62 kcal mol^{-1} and ΔE (*cis*-HONO^S *trans*-HONO^T) is 56.27 kcal mol^{-1}, respectively.

Cis to trans isomerization can also proceed under electronic excitation to *trans*-HONO with further quenching of excited molecules:

$$cis\text{-}^1\text{HONO} \rightarrow trans\text{-}^3\text{HONO} \rightarrow trans\text{-}^1\text{HONO}$$

$$trans\text{-}^1\text{HONO} \rightarrow trans\text{-}^3\text{HONO} \rightarrow trans\text{-}^1\text{HONO}$$

This phenomenon could explain the much faster cis–trans isomerization rate observed in some experiments, as compared to the opposite interconversion (vide supra).

This photoexcitation/conversion to the trans isomer may also have atmospheric implications explaining the abundance of isoenergetic trans isomer of HONO in the photochemistry studies on the atmospheric systems.

The triplet state flat structure of HNO$_2$ is not a minimum but a transition state for the pyramidalization with N−H bond deformation modes of 2931i cm^{-1} at B3LYP/6–31G(d,p) level. More detailed results on triplet state PES of HONO will be presented in future studies.

CONCLUSIONS

G3, CBS-QB3, and CBS-APNO calculation methods are used to determine thermochemical data for nitrous acid isomers, the simplest precursors of organic nitrites and nitro compounds. These values will be of value as reference to calculations on larger molecule, organic nitrogen oxide species.

The recommended ΔH_f^o (298 K) for *trans* nitrous acid is -18.9 ± 0.05, which is 0.46 kcal mol^{-1} more stable than the cis isomer and 8.0 kcal mol^{-1} than the HNO$_2$ structure at ΔH_f^o (298 K) $= -10.9$ kcal mol^{-1}.

HNO$_2$ is more reactive toward abstraction reactions because the H−NO$_2$ bond is some 8 kcal mol^{-1} weaker than the H−ONO bond, and HNO$_2$ does not have the weak (48.5 kcal mol^{-1}) HO−NO bond. HNO$_2$ can undergo isomerization with a similar barrier to the HO−NO bond cleavage; hence, it may serve as a source of OH radicals in photochemistry of the atmosphere. The isomerization has a lower pre-exponential factor, than HO−NO dissociation, so HNO$_2$ is slightly more stable to NO + OH formation from a thermal reaction.

APPENDIX A: ATOMIZATION ANALYSIS FOR ENTHALPY OF FORMATION

A1: Atomization Reaction and Thermal Corrections

Atomization energy [67,68] is used for determination of enthalpies at 0 and 298.15 K. Atomization energies, ΣD_0 were computed via

$$\Sigma D_0(H_x N_y O_z) = x E_0(\text{Theor, H}) + y E_0(\text{Theor, N})$$
$$+ z E_0(\text{Theor, O}) - E_0(\text{Theor}, H_x N_y O_z) \quad \text{(Eq. 1)}$$

using the composite calculation method energies and zero-point energy corrections (theoretical values at 0 K) for atoms and respective molecules.

Enthalpies of formation at 0 K were computed using experimental enthalpies of formation for atoms (Table I, second set) and calculated atomization energies.

$$\Delta H_f^o(H_x N_y O_z, 0 \text{ K}) = x \Delta H_f^o(H, \ 0 \text{ K})$$
$$+ y \Delta H_f^o(N, \ 0 \text{ K}) + z \Delta H_f^o(O, \ 0 \text{ K})$$
$$- \Sigma D_0(H_x N_y O_z, 0 \text{ K}) \quad \text{(Eq. 2)}$$

Temperature correction parameters (T_c) for the atoms to obtain $\Delta_f H^o$ (298.15 K) were taken from the literature [62] (parenthetical digits from Table I). The final formation enthalpy at 298.15 K is computed as follows:

$$\Delta H_f^o(H_x N_y O_z, 298.15 \text{ K}) = \Delta H_f^o(H_x N_y O_z, \ 0 \text{ K})$$
$$+ T_c(H_x N_y O_z) - x T_c(H) - y TC(N) - z T_c(O) \quad \text{(Eq. 3)}$$

$T_c(H_x N_y O_z)$ is a theoretical value of the temperature correction for molecule.

A2: Atomization Reaction to Enthalpy at 298 K

Calculations were also done using the following, simpler, scheme in which the enthalpies of formation at 298.15 K were obtained directly using (Eq. 4)

$$\Delta H_f^o(H_x N_y O_z, 298.15 \text{ K}) = x \Delta H_f^o(H, \ 298.15 \text{ K})$$
$$+ y \Delta H_f^o(N, 298.15 \text{ K}) + z \Delta H_f^o(O,$$
$$298.15 \text{ K}) - \Sigma D_0(H_x N_y O_z, 298.15 \text{ K}) \quad \text{(Eq. 4)}$$

Atomization energies (Eq. 1) were computed using enthalpy of reaction (in place of E_0) at 298.15 K and experimental heats of formation of constituent atoms

at the same temperature 298.15 K from NIST Webbook (Table I, first set). $\Delta_f H^o$ (298.15 K) for oxygen atom was corrected (reduced) by 0.125 kcal mol^{-1} to be consistent with the results of the conventional method (Eq. 3) [51, 79].

APPENDIX B: THERMAL-H$_{298}$ CORRECTION FOR HONO ISOMERS

The -1.51 kcal mol^{-1} thermal correction (0–298 K) for enthalpy of formation is from the CBS-QB3 method (see Table I). This value is close to calculated values of -1.51 to -1.56 kcal mol^{-1} determined by Bauerfeldt and coworkers [24]. This thermal energy was also evaluated by Chase [48] and by Gurvich et al. [49] as -1.49 and -1.52, respectively, for the cis isomer, and -1.47 kcal/mol for the trans isomer.

In the above text and discussion, we convert all zero Kelvin values of $\Delta_f H^o$ from [19b] to $\Delta_f H_{298}^o$ by use of this -1.51 kcal mol^{-1} correction, in order to be consistent in the comparison of the various enthalpy data.

BIBLIOGRAPHY

1. (a) Stemmler, K.; Ammann, M.; Donders, C.; Kleffmann, J.; George, C. Nature 2006, 440, 195–198; (b) Finlayson-Pitts, B. J.; Pitts, J. N., Jr., Chemistry of the Upper and Lower Atmosphere: Theory, Experiments and Applications; Academic Press: San Diego, CA, 2000; (c) Miller, Y.; Chaban, G. M.; Finlayson-Pitts, B. J.; Gerber, R. B. J Phys Chem A 2006, 110, 5342–5354.

2. (a) Acker, K.; Febo, A.; Trick, S.; Perrino, C.; Bruno, P.; Wiesen, P.; Möller, D.; Wieprecht, W.; Auel, R.; Giusto, M.; Geyer, A.; Platt, U.; Allegrini, I. Atmos Environ 2006, 40, 3123–3133; (b) Calvert, J. G.; Yarwood, G.; Dunker, A. M. Res Chem Intermed 1994, 20, 463–452; (c) Lammel, G.; Cape, J. N. Chem Soc Rev 1996, 25, 361–369.

3. Gerecke, A.; Thielmann, A.; Gutzwiller, L.; Rossi. M. J. Geophys Res Lett 1998, 25, 2453–2456.

4. Rondon, A.; Sanhueza, E. Tellus B 1988, 41, 474–477.

5. March, J. Advanced Organic Chemistry, Reaction Mechanism, and Structure: 4th ed.; Wiley: New York, 1992.

6. (a) Loeppky, R. N. Nitrosamine and N-Nitroso Compound Chemistry and Biochemistry Advances and Perspectives. In Nitrosamines and Related N-Nitroso

Compounds; Loeppky, R. N., Michejda, C. J. (Eds.); American Chemical Society Symposium Series, 553; Washington, DC: American Chemical Society, 1994.; pp. 1–18, 52–65; (b) Olderive, C.; Zhao, K.; Paganga, G.; Halliwell, B.; Rice-Evand, C. Chem Res Toxicol 1998, 11, 1574–1579.

7. Jarvis, D. L.; Leaderer, B. P.; Chinn, S.; Burney, P. G. Thorax 2005, 60, 474–479.

8. Arens, F.; Amman, M.; Gutzwiller, L.; Baltensperger, U.; Gäggeler, H. W. J Aerosol Sci 2000, 31, S1035.

9. Finlayson-Pitts, B. J.; Pitts, J. N. Science 1997, 276, 1045–1052.

10. Koch, T. G.; Sodeau, J. R. P. J Phys Chem 1995, 99, 10824–10829.

11. (a) Tsang, W.; Herron, J. T. J Phys Chem Ref Data 1991, 20, 609–663; (b) Fifer, R. A. J Phys Chem 1976, 80, 2717–2723.

12. (a) Brill, T. B. In Chemistry and Physics of Energetic Materials; Bulusu, S. (Ed.); Kluwer: Dordrecht, the Netherlands, 1990; p. 277; (b) Clothier, P. Q. E.; Aguda, B. D.; Moise, A.; Pritchard, H. O. Chem Soc Rev 1993, 22, 101; (c) Chan, W. -T.; Heck, S. M.; Pritchard, H.O. Phys Chem Chem Phys 2001, 3, 56.

13. Vasudev, R.; Zare, R. Z.; Dixon, R. J Chem Phys 1983, 96, 399–402.

14. Amaral, G.; Xu, K.; Zhang, J. J Phys Chem A 2001, 105, 1465–1475.

15. Kuo, K. K.; Summerfield, M. Fundamentals of Solid Propellant Combustion, Progress in Astronautics and Aeronautics; AIAA: New York, 1984; Vol. 90.

16. Dean, A. M.; Bozzelli, J. W. In Gas-Phase Combustion Chemistry; Gardiner, W. C., Jr. (Ed.); Springer: New York, 1999; pp. 125–341.

17. Alexander, M. H.; Dagdigian, P. J.; Jacox, M. E.; Kolb, C. E.; Melius, C. F. Prog Energy Combust Sci 1991, 17, 263–296.

18. (a) Farnell, L.; Ogilvie, J.F. Proc R Soc London Ser A 1982, 381, 443–455; (b) Baldeschwieler, J. D.; Pimentel, G. C. J Chem Phys 1960, 33, 1008–1015; (c) Hall, R. J.; Pimentel, G. C. J Chem Phys 1963, 38, 1889.

19. (a) Jursic, B. S. Chem Phys Lett 1999, 299, 334–344; (b) Jursic, B. S. J Mol Struct (Theochem) 1999, 492, 35–43.

20. (a) Chan, W.-T.; Pritchard, H. O. Phys Chem Chem Phys 2002, 4, 557–560; (b) Chan, W.-T.; Heck, S. M.; Pritchard, H. O. Phys Chem Chem Phys 2001, 3, 56–62.

21. Sengupta, D.; Sumathi, R.; Peyerimhoff, S. D. Chem Phys 1999, 248, 147–159.

22. Sumathi, R.; Ashcraft, R. W.; Vial, M.; Klasky, M. L. J Phys Chem A 2005, 109, 8526–8536.

23. Nguyen, M. T.; Sumathi, R.; Sengupta, D.; Peeters, J. Chem Phys 1998, 230, 1–11.

24. Bauerfeldt, G. F.; Arbilla, G.; da Silva, E. C. J Braz Chem Soc 2005, 16, 190–196.

25. Wu, H.; Glaser, R. J Phys Chem A 2003, 107, 11112–11119.

26. Gutsev, G. L.; Jena, P.; Bartlett, R. J Chem Phys 1999, 110, 403–411.

27. (a) Mebel, A. M.; Lin, M. C.; Melius, C. F. J Phys Chem A 1998, 102, 1803–1807; (b) Lu, X.; Park, J.; Lin, M.C. J Phys Chem 2000, 104, 8730–8738; (c) Mebel, A. M.; Diau, E. W. G.; Lin, M. C.; Morokuma, K. J Phys Chem 1996, 100, 7517–7525; (d) Yamaguchi, Y.; Teng, Y.; Shimomura, S.; Tabata, K.; Suzuki, E. J Phys Chem A 1999, 103, 8272–8278.

28. (a) McGraw, G. E.; Bernitt, D. L.; Hisatsune, I. C. J Chem Phys 1966, 45, 1392 and 1966; (b) Deeley, C. M.; Mills, I. M. J Mol Struct 1983, 100, 199–213.

29. Varma, R.; Curl, R. F. J Phys Chem 1976, 80, 402–409.

30. (a) Finnigan, D. J.; Cox, A. P.; Brittain, A. H. J Chem Soc, Faraday Trans 2 1972, 68, 548–565; (b) Cox, A. P.; Brittain, A. H.; Finnigan, D. J. Trans Faraday Soc 1971, 67, 2179–2194.

31. Lohre, L. L.; Barker, J. R.; Shroll, R. M. J Phys Chem A 2003, 107, 7429–7433.

32. (a) Cox, A. P.; Kuczkowski, R. L. J Am Chem Soc 1966, 88, 5071–5074; (b) Cox, A. P.; Ellis, M. C.; Attfield, C. J.; Ferris, A. C. J Mol Struct 1994, 320, 91–106.

33. Greenwood, N. N.; Earnshaw, A. Chemistry of the Elements; Butterworth-Heinemann: Oxford, 1997.

34. Ling, P.; Boldyrev, A. I.; Simons, J.; Wight, C. A. J Am Chem Soc 1998, 120, 12327–12333.

35. Jursic, B. S. Int J Quant Chem 1996, 58, 41–46.

36. (a) DeKock, R. L.; McGuire, M. J.; Piecuch, P.; Allen, W. D.; Schaefer, H. F., III; Kowalski, K.; Kucharski, S. A.; Musial, M.; Bonner, A. R.; Spronk, S. A.; Lawson, D. B.; Laursen, S. L. J Phys Chem A 2004, 108, 2893–2903; (b) Laursen, S. L.; Grace, J. E., Jr.; DeKock, R. L.; Spronk, S. A. J Am Chem Soc 1998, 120, 12583–12594.

37. (a) Melius, C. F. BAC-MP4 Calculated Heats of Formation at 298K; Sandia National Laboratories, Livermore, 1997; (b) Miller, J. A.; Melius, C. F. Proc Combust Inst 1992, 24, 719–726.

38. (a) Fueno, T.; Yokayama, K.; Takane, S.-Ya. Theor Chim Acta 1992, 82, 299–308; (b) Yamaguchi, K.; Yabushita, S.; Fueno, T. J Chem Phys 1979, 71, 2321–2322; (c) Čižek, J.; Paldus, J. J Chem Phys 1967, 47, 3976; (d) Fukutome, H. Progr Theor Phys 1968, 40, 998.

39. Takane, S.Y.; Fueno, T. Theor Chim Acta 1994, 87, 431–439.

40. (a) Nakamura, S.; Takahashi, M.; Okazaki, R.; Morokuma, K. J Am Chem Soc 1987, 109, 4142–4148; (b) Kahn, S. D.; Hehre, W. J.; Pople, J.A. J Am Chem Soc 1987, 109, 1871–1873; (c) McKee, M.L. J Phys Chem 1989, 93, 7365–7369; (d) Hiberty, P. C.; Ohanessian, G., J Am Chem Soc 1982, 104, 66–70.

41. (a) Richter, F.; Rosmus, P.; Gatti, F.; Meyer, H-D. J Chem Phys 2004, 120, 6072–6084; (b) Qin, Y.; Thompson, D. L. J Chem Phys 1994, 100, 6445–6457; (c) Guo, Y.; Thompson, D. L. J Chem Phys 2003, 118, 1673–1678.

42. De Maré, G. R.; Moussaoui, Y. Int Rev Phys Chem 1999, 18, 91–117.

43. (a) Shirk, A. E.; Shirk, J. S. Chem Phys Lett 1983, 97, 549–552; (b) McDonald, P. A.; Shirk, J. S. J Chem Phys 1982, 77, 2355–2364.

44. Reiche, F.; Abel, B.; Beck, R. D.; Rizzo, T. R. J Chem Phys 2000, 112, 8885–8898.

45. Francisco, J. S. J Chem Phys 2001, 115, 2117–2122.

46. http://webbook.nist.gov/chemistry.

47. Dransfield, T. J.; Donahue, N. M.; Anderson, J. G. J Phys Chem A 2001, 105, 1507–1514.

48. Chase, M. W., Jr. NIST–JANAF Themochemical Tables, 4th ed. J Phys Chem Ref Data, Monograph 9, 1998, 1–1951.

49. Gurvich, L. V.; Veyts, I. V.; Alcock, C. B. Thermodynamic Properties of Individual Substances, 4th ed.; Hemisphere Publishing: New York, 1991; Vol. 2.

50. Benson, S. W. Thermochemical Kinetics, 2nd ed.; Wiley: New York, 1976.

51. Asatryan, R.; Bozzelli, J. W.; Simmie, J. M. Thermochemistry of Methyl and Ethyl Nitro, RNO2, and Nitrite, RONO, Organic Compounds. To be submitted.

52. da Silva, G.; Bozzelli, J. W.; Sebbar, N.; Bockhorn, H. ChemPhysChem 2006,7, 1119.

53. Mebel, A. M.; Lin, M.C.; Morokuma, K.; Melius, C. F. J Phys Chem 1995, 99, 6842–6848.

54. Zhao, H.; Liu, K.; Ma, S.; Li, Z. Int J Quant Chem 2005, 101, 113–117.

55. Hug, G. L.; Camaioni, D. M.; Carmichael, I. J Phys Chem A 2004, 108, 6599–6604.

56. Guillory, W. A.; Hunter, C. E. J Chem Phys 1971, 54, 598–603.

57. Walsh, A. D. J Chem Soc 1953, 2266–2288.

58. (a) Kee, R. J.; Rupley, F. M.; Meeks, E.; Miller, J. A. CHEMKIN-III: A Fortran Chemical Kinetics Package for the Analysis of Gas-Phase Chemical and Plasma Kinetics; Report UC-405, SAND96-8216, Sandia National Laboratories, Livermore, CA , 1996; (b) Bromly, J. H.; Barnes, F. J.; Muris, S.; You, X.; Haynes, B. S. Comb Sci Technol 1996, 115, 259–297; (c) Mereac, G.; Dagaut, P.; Roesler, J. F.; Cathonnet, M. Combust Flame 2006, 145, 512–520; (d) Djurisic, Z. M. PhD Thesis, University of Utah, 2004.

59. Montgomery, J. A., Jr.; Frisch, M. J.; Ochterski, J. W.; Petersson, G. A. J Chem Phys 1999, 110, 2822–2827.

60. Montgomery, J. A., Jr.; Ochterski, J. W.; Petersson, G. A. J Chem Phys 1994, 101, 5900–5909.

61. Curtiss, L. A.; Raghavachari, K.; Redfern, P. C.; Rassolov, V.; Pople, J. A. J Chem Phys 1998, 109, 7764–7776.

62. Gaussian 03, Revision D.01. Frisch, M. J.; Trucks, G. W.; Schlegel, H. B.; Scuseria, G. E.; Robb, M. A.; Cheeseman, J. R.; Montgomery, J. A., Jr.; Vreven, T.; Kudin, K. N.; Burant, J. C.; Millam, J. M.; Iyengar, S. S.; Tomasi, J.; Barone, V.; Mennucci, B.; Cossi, M.; Scalmani, G.; Rega, N.; Petersson, G. A.; Nakatsuji, H.; Hada, M.; Ehara, M.; Toyota, K.; Fukuda, R.; Hasegawa, J.; Ishida, M.; Nakajima, T.; Honda, Y.; Kitao, O.; Nakai, H.; Klene, M.; Li, X.; Knox, J. E.; Hratchian, H. P.; Cross, J. B.; Adamo, C.; Jaramillo, J.; Gomperts, R.; Stratmann, R. E.; Yazyev, O.; Austin, A. J.; Cammi, R.; Pomelli, C.; Ochterski, J. W.; Ayala, P. Y.; Morokuma, K.; Voth, G. A.; Salvador, P.; Dannenberg, J. J.; Zakrzewski, V. G.; Dapprich, S.; Daniels, A. D.;

Strain, M. C.; Farkas, O.; Malick, D. K.; Rabuck, A. D.; Raghavachari, K.; Foresman, J. B.; Ortiz, J. V.; Cui, Q.; Baboul, A. G.; Clifford, S.; Cioslowski, J.; Stefanov, B. B.; Liu, G.; Liashenko, A.; Piskorz, P.; Komaromi, I.; Martin, R. L.; Fox, D. J.; Keith, T.; Al-Laham, M. A.; Peng, C. Y.; Nanayakkara, A.; Challacombe, M.; Gill, P. M. W.; Johnson, B.; Chen, W.; Wong, M. W.; Gonzalez, C.; Pople, J. A. Gaussian, Inc., Pittsburgh, PA, 2003.

63. Cramer, C. J. Essentials of Computational Chemistry: Theories and Methods; Wiley: New York, 2002.

64. Mayer, P. M.; Parkinson, C. J.; Smith, D. M.; Radom, L. J Chem Phys 1998, 108, 604–615.

65. Sheng, C. Ph.D. dissertation, Department of Chemical Engineering, New Jersey Institute of Technology, Newark, NJ, 2002.

66. Curtiss, L. A.; Raghavachari, K.; Redfern, P. C.; Pople, J. A. J Chem Phys 1997, 106, 1063–1079.

67. Ochterski, J. W. Thermochemistry in Gaussian, Gaussian Inc., Pittsburgh, PA, 2000.

68. Nikolaidis, A.; Rauk, A.; Glukhovtsev, M. N.; Radom, L. J Phys Chem 1996, 100, 17460–17564.

69. Ruscic, B.; Boggs, J. E.; Burcat, A.; Csaszar, A. G.; Demaison, J; Janoschek, R.; Martin, J.M.L.; Morton, M.L.; Rossi, M.J.; Stanton, J.F.; Szalay, P.G.; Westmoreland, P.R.; Zabel, F.; Berces, T. J Phys Chem Ref Data 2005, 34, 573– 656.

70. Dixon, D.A.; Francisco, J.S.; Alexeev, Y. J Phys Chem A 2006, 110, 185–191.

71. Anderson, W. R. Combust Flame 1999, 117, 394–403.

72. Frenkel, M.; Kabo, G. J.; Marsh, K. N.; Roganov, G. N.; Wilhoit, R. C. Thermodynamics of Organic Compounds in the Gas State; Thermodynamics Research Center: College Station, TX, 1994; Vol. I.

73. Pedley, J. B. Thermochemicsl Data and Structures of Organic Compounds; Thermodynamics Data Center: College Station, TX, 1994.

74. Stull, D. R.; Westrum, E. F.; Sinke, G. C. The Chemical Thermodynamics of Organic Compounds; Wiley: New York, 1969.

75. Cox, J. D.; Wagman, D. D.; Medvedev, V. A., CODATA Key Values for Thermodynamics; Hemisphere Publishing; New York, 1984, 1.

76. Ruscic, B.; Pinzon, R. E.; Morton, M. L.; Srinivasan, N. K.; Su, M.-C.; Sutherland, J. W.; Michael, J.V. J Phys Chem A 2006, 110, 6592.

77. (a) Sheng, Chad PhD Thesis NJIT (2001) THERMKIN code; (b) Ritter, E. R., Bozzelli, J. W. Int J Chem Kinet 1991, 23, 767. THERM code

78. Greenblatt, G.D.; Howard, C.J. J Phys Chem 1989, 93, 1035–1042.

79. da Silva, G.; Asatryan, R.; Rutz, L.; Bozzelli, J. W. Manuscript in preparation.

80. Cox, J. D.; Pilcher, G. Thermochemistry of Organic and Organometallic Compounds; Academic Press: New York, 1970, p. 310.